AD NUMBER

AD803397

LIMITATION CHANGES

TO:

Approved for public release; distribution is unlimited.

FROM:

**Distribution authorized to U.S. Gov't. agencies and their contractors;
Administrative/Operational Use; OCT 1966. Other requests shall be referred to Rome Air Development Center, Griffiss AFB, NY.**

AUTHORITY

RADC ltr 17 Sep 1971

RADC-TR-66-506
Final Report

HIGH POWER S-BAND ELECTRON BEAM PHASE SHIFTER TECHNIQUE

Dr. Grant St John

Raytheon Company

TECHNICAL REPORT NO. RADC-TR-66-506
October 1966

Rome Air Development Center
Research and Technology Division
Air Force Systems Command
Griffiss Air Force Base, New York

HIGH POWER S-BAND ELECTRON BEAM PHASE SHIFTER TECHNIQUE

Dr. Grant St John

Raytheon Company

Bedford General Design Company, Bedford, 17 November 1966, 140 copies

FOREWORD

This final technical report was prepared by Dr. Grant St. John of Raytheon Company, Microwave and Power Tube Division, Waltham, Massachusetts, under contract AF 30(602)-3663, Project 4506, Task No. 450602. The secondary report number is PT-1101. The RADC Project Engineer was Mr. Ronald W. Vandivier, EMATE.

This report covers a period of work performed from 15 March 1965 to 15 July 1966.

Release of subject report to the general public is prohibited by the Strategic Trade Control Program, Mutual Defense Assistance Control List (revised 6 January 1965) published by the Department of State.

This report has been reviewed and is approved.

Approved: RONALD W. VANDIVIER
Project Engineer
Electron Devices Section

Approved: THOMAS S. BOND, JR
Colonel, USAF
Chief, Surveillance & Control Division

FOR THE COMMANDER:
IRVING J. GABELMAN
Chief, Advanced Studies Group

ABSTRACT

This report is a summary of work performed under the sponsorship of Rome Air Development Center (Contract AF30(602)-3663) to design and develop a breadboard model of a 100 kilowatt S-band phase shifter. The phase shifter utilizes an electron beam of input power much lower than the microwave power transmitted through the structure. The variable current beam interacts with the slow-wave structure to perturb the propagation constants of the combined beam and slow-wave structure system.

A model was constructed and operated at a 100 kilowatt power level. The performance of this model was limited by low beam current; however, measured performance was in excellent agreement with theoretical values.

From this work, it can be concluded that a device in S-band operating at a 100 kilowatt power level and providing 360^{o} variation in phase shift is feasible. The physical size and relatively high insertion loss of such an electron beam phase shifter tend to make it unattractive in comparison with recently developed solid-state phase shifters.

TABLE OF CONTENTS

LIST OF ILLUSTRATIONS

1.0 INTRODUCTION

In 1962, Raytheon Company demonstrated that variation of electron beam current would produce a variable phase shift characteristic in a slow-wave structure at a low ratio of phase shift control power to electron beam power. A study program was initiated in July 1963 and completed in August 1964 under the sponsorship of Rome Air Development Center (Contract AF30(602)-3161). On March 15, 1965, Raytheon was awarded a contract by RADC (AF30(602)-3663) to design and develop a breadboard model of a 100-kilowatt S-band phase shifter using the results of the initial contract as a starting point. The device is shown in Figure 1-1.

During the first phase shifter program the theoretical study was carried out. First an appropriate solution of Maxwell's equation was employed to predict phase shift to within a constant value. Because of the complexity of the solution, the constant was determined experimentally on three widely different models, and excellent agreement (within 10%) was attained. Secondly, in a parallel effort, a computer program was set up to solve the individual electron trajectories which, by evaluation of the electron beam currents, could determine phase shift. Results were attained for a single combination of parameters.

The results of this program were used to design a phase shifter meeting the requirements of RADC Purchase Request No. 65-209.* As outlined in Raytheon's proposal (PRP1230-2), the combination of 100 kw peak rf power, 360 degrees phase shift, 0.5 db insertion loss, and permanent magnet focusing dictated a method of approach. The electron beampower level was determined by utilizing the specified phase control power (maximum of 1/5th of the microwave power) coupled with a reasonable degree of collector depression. Permanent magnet focusing of this level of beam power, within a 3.0 - 3.3 GHz slow-wave structure forced utilization of a high perveance hollow electron beam, injected into a slow-wave structure of propagation constant $\gamma_a \approx 3.3$.

*See Appendix A.

Figure 1-1 100 Kilowatt S-Band Phase Shifter QR1242 - Breadboard Model

This large beam diameter and slow-wave circuit beam aperture resulted in an area in which extrapolation of the phase shift theory had to be taken with a certain degree of precaution, since no experimental information was available. Furthermore, no data were available to indicate the effect on slow-wave circuit coupling impedance using such a large beam aperture. With these potential problem areas anticipated, the program was initiated.

2.0 DESIGN APPROACH

During an earlier program[1,2] an expression for the incremental change in phase shift through an electron beam loaded slow-wave structure was derived and experimentally verified. This equation is

$$\Delta\theta = a\, I_o\, Lf \sqrt{\frac{K}{V_o P_{rf}}} \qquad (1)$$

where

- $\Delta\theta$ = Phase shift in radians
- a = Empirically determined constant = 20
- I_o = Electron beam current in amperes
- L = Length of slow wave circuit in centimeters
- f = Frequency in GHz/sec
- K = Slow-wave circuit coupling impedance in ohms
- V_o = Beam voltage in volts
- P_{rf} = Rf power on the slow-wave circuit in watts

An alternative form to equation (1), which is useful for discussion, is

$$\Delta\theta = a'\, C^{3/2}\, N \sqrt{\frac{P_b}{P_{rf}}} \qquad (2)$$

where

$$C = \left(\frac{K I_o}{4 V_o}\right)^{1/3} = \text{Pierce's}^{3} \text{ gain parameter} \qquad (3)$$

- N = Number of circuit guide wavelengths
- P_b = $I_o V_o$ = beam power in watts
- a' = 149 = a multiplied by physical constants.

It is important to remember that equation (2) determines phase shift only in the phase shifter type mode of operation (rf power on the circuit greater than dc beam power).

The design approach, as per equation (2) is as follows:

a. At maximum phase shift let the beam power equal the rf circuit power. This will guarantee the linear phase vs beam current characteristic while minimizing beam power. Therefore, the beam power is 100 kw.

b. Circuit length, N, is to be a compromise between being high to achieve the phase shift but low to achieve a short circuit length to minimize size and weight.

c. Maximize the gain parameter C. This goal implies usage of the highest rf circuit coupling impedance and electron beam perveance.

The requirement of 0.5 db maximum rf insertion loss eliminates usage of a helix. The 3.0 - 3.3 GHz operating bandwidth lends itself admirably to a periodic type of slow-wave structure such as a coupled cavity circuit. This choice compromises the higher coupling impedance of the helix for the lower rf insertion loss of the coupled cavity circuit.

The magnetic field was set at 600 gauss to assure the capability of permanent magnet focusing, although this breadboard model is to be solenoid focused.

The collector was designed to be consistent with a high level of collector depression. If the phase control power is to be a maximum of 1/5 of the rf power, and the beam power is to equal the rf power, a high degree of collector depression is required.

The phase shifter will be operating at 180 degrees phase shift, on the average, where only half the maximum beam power is required, since phase shift is proportional to beam current. Therefore, the collector depression is to be consistent with 2/5 of the maximum beam power, or 40 kw peak of collector plus rf circuit dissipation, at maximum phase shift.

3.0 ELECTRON BEAM AND GUN

The electron beam was chosen to be $V_o = 10$ kV and $I_o = 10$ amperes, giving the required 100 kw at the relatively high but readily achievable value of beam perveance of 10 microperves. To focus this beam in a magnetic field of 600 gauss require designing for a 400 gauss Brillouin field. The maximum beam current density is then

$$J_o = \left[\frac{B_b V_o^{1/4}}{1472}\right]^2 = \left[\frac{400\,(10,000)^{1/4}}{1472}\right]^2 = 7.35 \ \frac{\text{amperes}}{\text{cm}^2} \qquad (4)$$

Fortunately, this is a high but reasonable cathode current density for pulsed operation. A nonconvergent electron gun is therefore suitable. A tubular electron beam with OD and ID of 1.60 and 0.91 cm, respectively, was chosen, since this produced a cross-sectional area consistent with the 7.35 amperes cm^2 and total current of 10 amperes as well as a perveance per square of 0.875 microperves/square. At this point, an estimate of the maximum velocity spread which could be tolerated in the beam was required. Dunn[4] gives the ratio of maximum and minimum beam velocities, (1 - p), as:

$$1 - p \cong \frac{4}{70} \ (S_\square \times 10^6) \qquad (5)$$

or $$1 - p = \frac{4}{70} \ (0.875) = 0.05$$

Later it will be shown that $C \approx 0.1$. Dunn gives two methods of estimating the maximum velocity spread before meaningful gain loss in a TWT. These indicate p should be less than 6% and/or p less than C. It was not clear at this time that either of these criteria were directly applicable but at least it supplied a probable benchmark. The validity of this early estimate is borne out by the results shown in Figures 7-3 and 7-5 of Appendix C. A reduction in velocity spread could have been achieved by an increase in electron beam diameter, while holding beam area constant. This would reduce beam perveance per square, $S_\square$, at the expense of a reduced coupling impedance.

The gun is a parallel plane triode with an intercepting mesh grid. The design is based on the work of Spangenberg[5] and Wolkstein.[6] The design parameters are shown in Table 3-1. The gun is gridded so that the phase shifter may be operated by dc high voltage supplies. Modulation may then be applied to the grid at relatively low voltage and current. The advantages of grid pulsing over usage of cathode pulsing are:

a. Cathode pulsing requires a 10 kv, 10 amp pulse capability. Grid pulsing requires only a 405 volt peak pulse at 1.7 amperes, a 50 volt grid bias supply, and a 10 kv dc cathode supply. In the former case, modulation is superimposed on the 10 kv pulse; while, in the grid modulation, the modulation is superimposed on the 405 volt pulse. The simplification in circuitry is therefore considerable.

b. In cathode pulsing, especially with periodic type structures such as the coupled cavity circuit, oscillations are seen on the rise and fall portions of the voltage pulse. This is due to synchronism with higher order slow-wave circuit space harmonics at the lower beam voltages. This problem is sidestepped in grid pulsing since beam voltage is fixed, but beam current is pulsed.

TABLE 3-1

Electron Gun Design Parameters

V_o	= 10 kV	d_{kg}	= 0.018 inch
I_o	= 10 amperes	d_{ka}	= 0.218 inch
J_k	= 7.35 amperes/cm^2	zr_g	= 0.0017 inch
Vg_{co}	= -55 volts,	d	= 0.020 inch
V_g	= 405 volts	r_b	= 0.315 inch
I_g	= 1.7 amperes		

Cathode - oxide coated

Grid - gold plated molybdenum wire mesh.

The cathode is an active nickel body sprayed with a triple carbonate coating. The heater is a serpentine wound tungsten wire utilizing a standard Raytheon heater support.

The ceramic heater supports trap the heater mechanically, producing a rugged heater design with complete assurance of freedom of heater-to-cathode short circuits. The grid is a standard 0.0017 inch diameter gold plated molybdenum wire mesh of 50 wires per inch. This mesh is brazed to a copper grid support ring which produces both a firm support and heat sink for the grid. The anode is a 0.015 inch thick molybdenum washer which has been photoetched by Raytheon's Materials and Techniques Group. The anode washer is brazed to a copper support ring.

Figure 3-1 shows heater current and cathode temperature vs heater voltage.

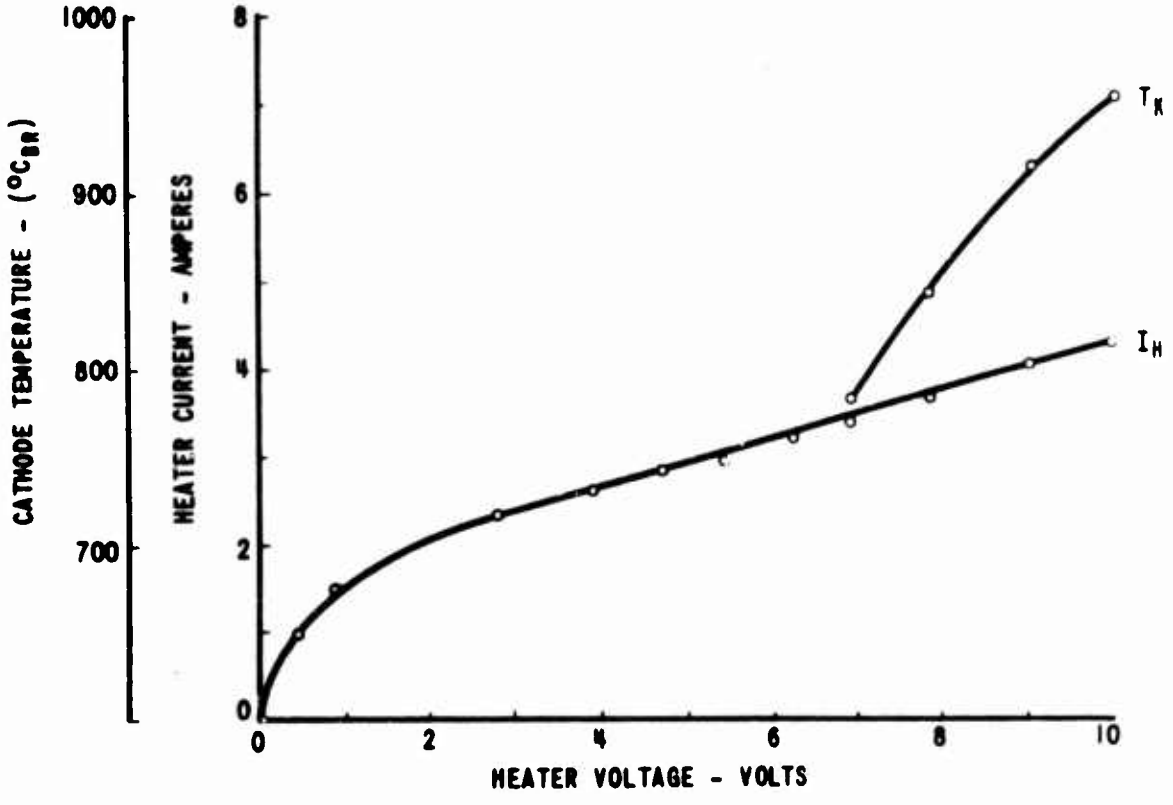

FIGURE 3-1 QR1242 Heater Characteristic

4.0 SLOW-WAVE CIRCUIT

The coupled cavity slow-wave circuit was selected because of its low insertion loss as well as its expected capability to supply adequate bandwidth and coupling impedance. As indicated previously, the focusing and beam power requirements dictated use of a large electron beam diameter and therefore large beam aperture in the circuit. To evaluate the effect of this large aperture and evolve a circuit design, a cold test phase was undertaken. The coupled cavity geometry is defined in Figure 4-1. The beam aperture radius was designed to accommodate the electron beam described in section 3.0, with a beam radius to aperture radius, $r_b/r_1 = 0.8$. The circuit period was adjusted for beam synchronism with the circuit wave. Evaluation of coupling hole size was evaluated experimentally. The circuit ω-β diagram[7] and variation of phase and group velocities vs frequency with change in coupling hole size are shown in Figures 4-2 to 4-4. The coupled cavity circuit described in Table 4-1 with an 85° coupling hole angle, covered the frequency range. A circuit bandwidth which is wider than operating bandwidth is desirable so that rf matching difficulties and the increased circuit loss, both obtained near circuit band edges, because of the low group velocity, are avoided.

TABLE 4-1

Coupled Cavity Circuit Dimensions

r_1	= 0.393 inch	r_5	= 0.125 inch
r_2	= 0.527 inch	g	= 0.106 inch
r_3	= 0.928 inch	t	= 0.196 inch
r_4	= 0.728 inch	α	= 85 degrees

Note: Dimensions defined in Figure 4-1.

The coupling impedance of this circuit was evaluated by means of dielectric rod perturbation techniques.[8] The coupling impedance vs frequency, as shown in Figure 4-5, varies from 20-43 ohms, as evaluated at $r = r_1$.

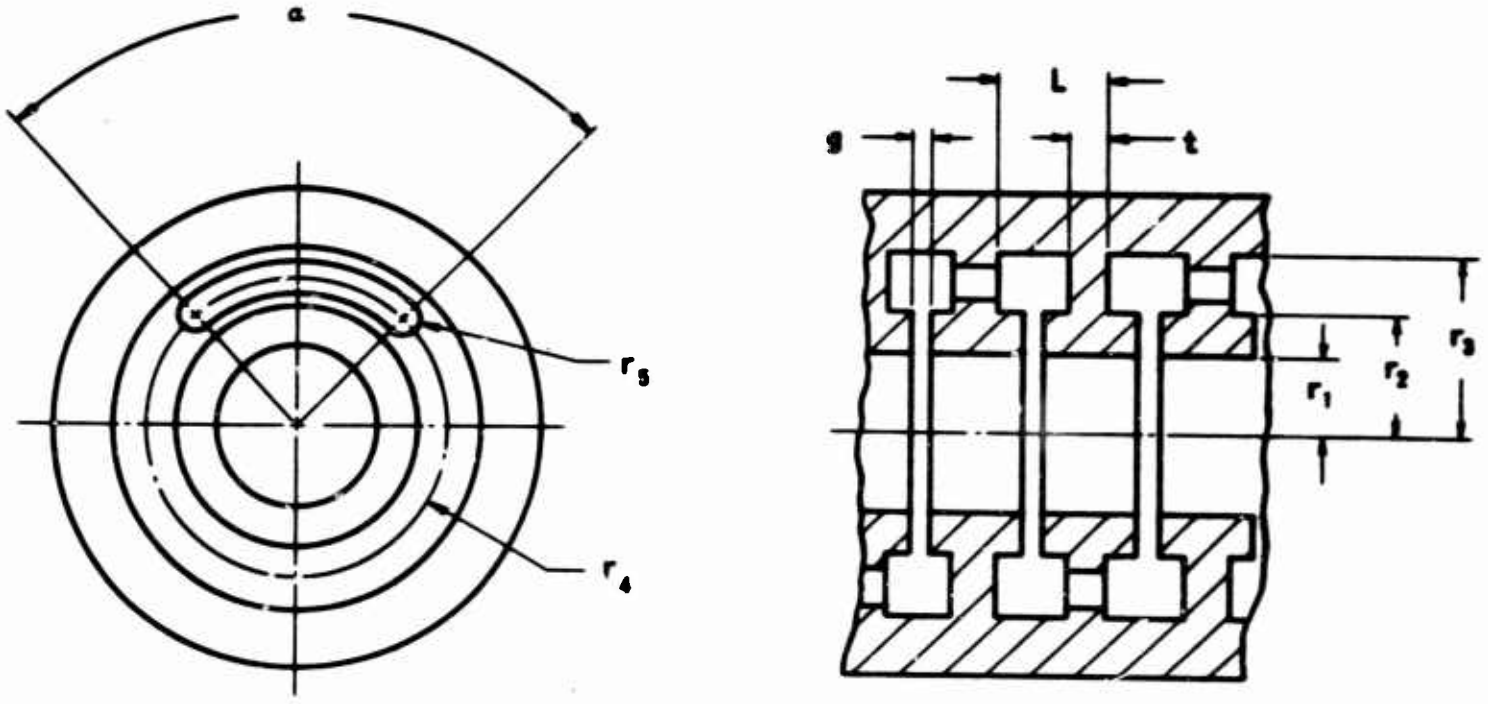

FIGURE 4.1 Coupled Cavity Circuit

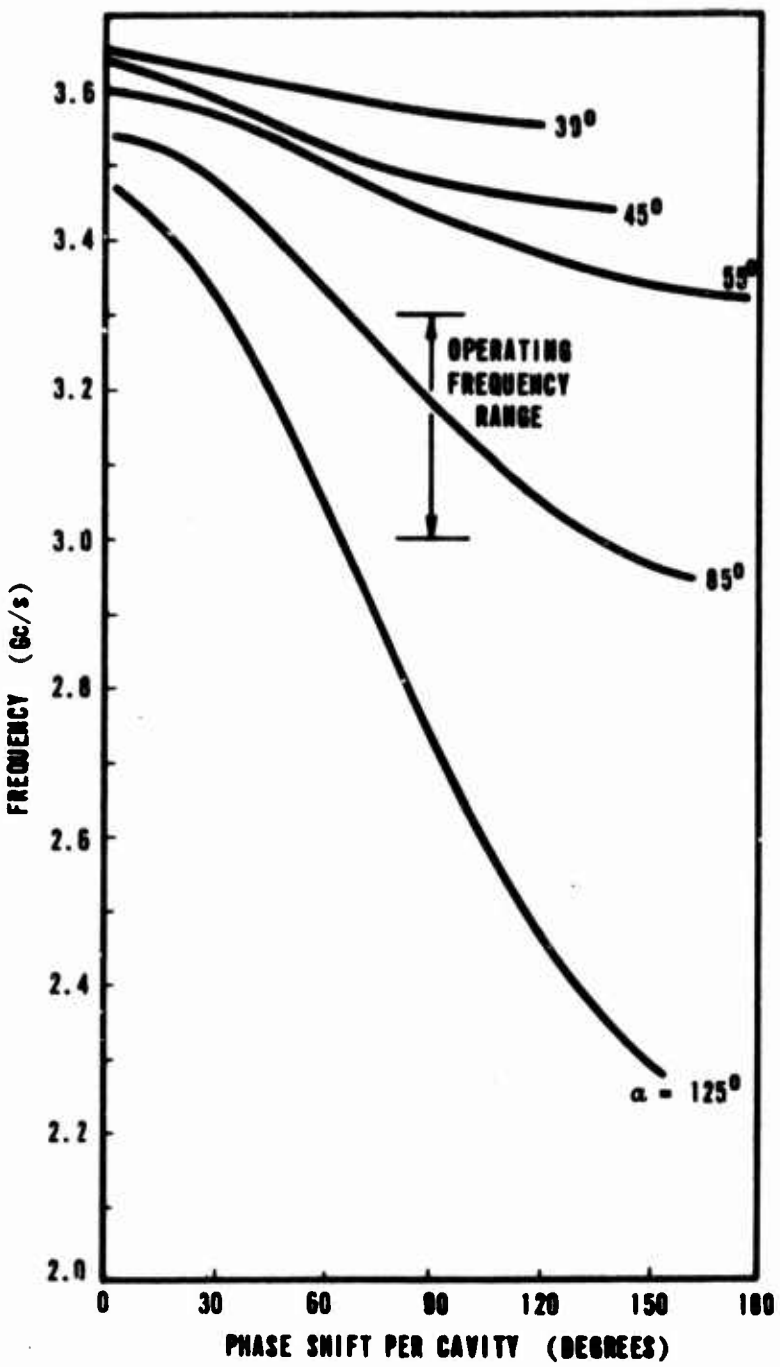

Figure 4-2 QR1242 Cold Test Structure

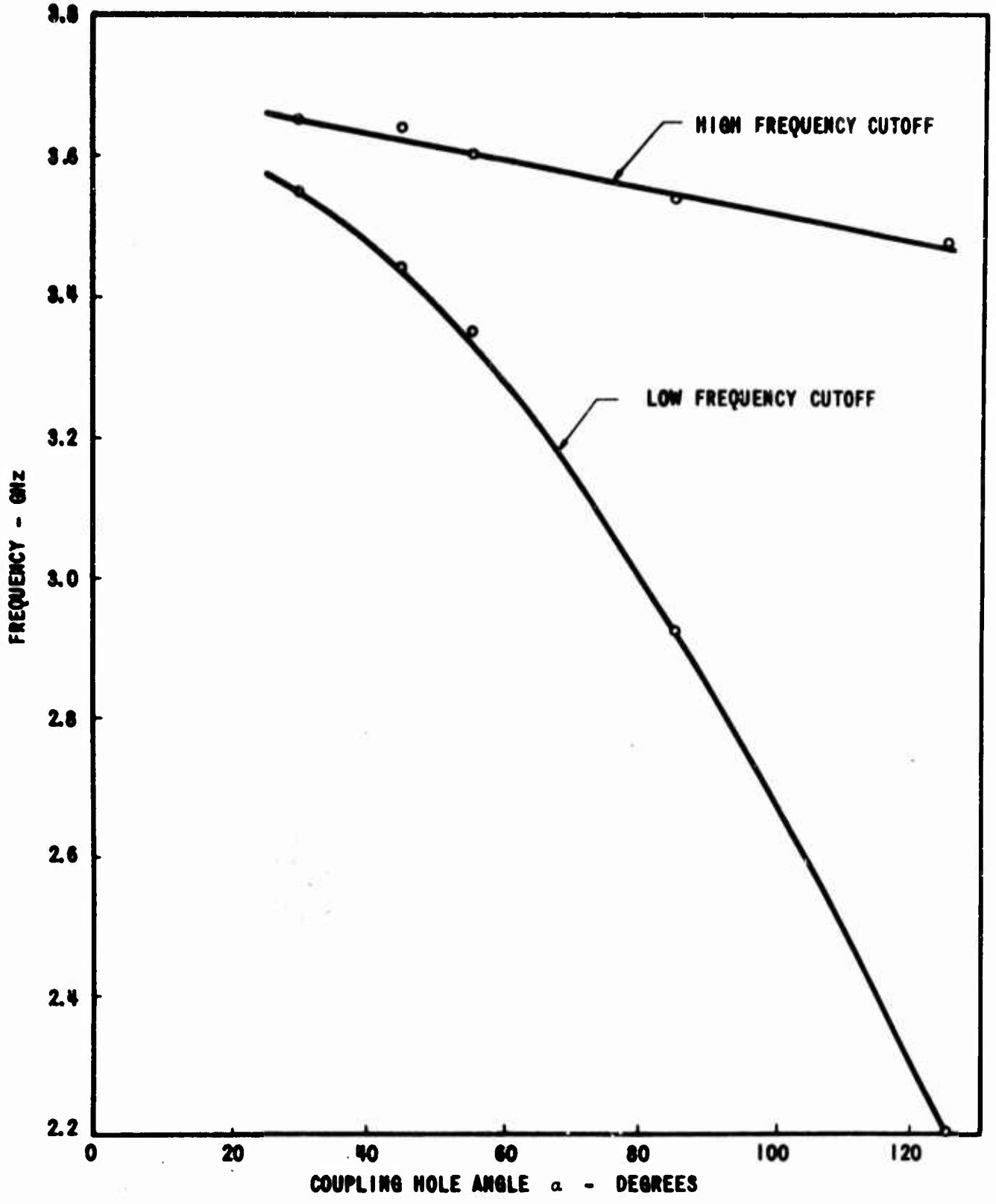

FIGURE 4-3 Coupled Cavity Circuit
Cutoff Frequencies vs Coupling Hole Size

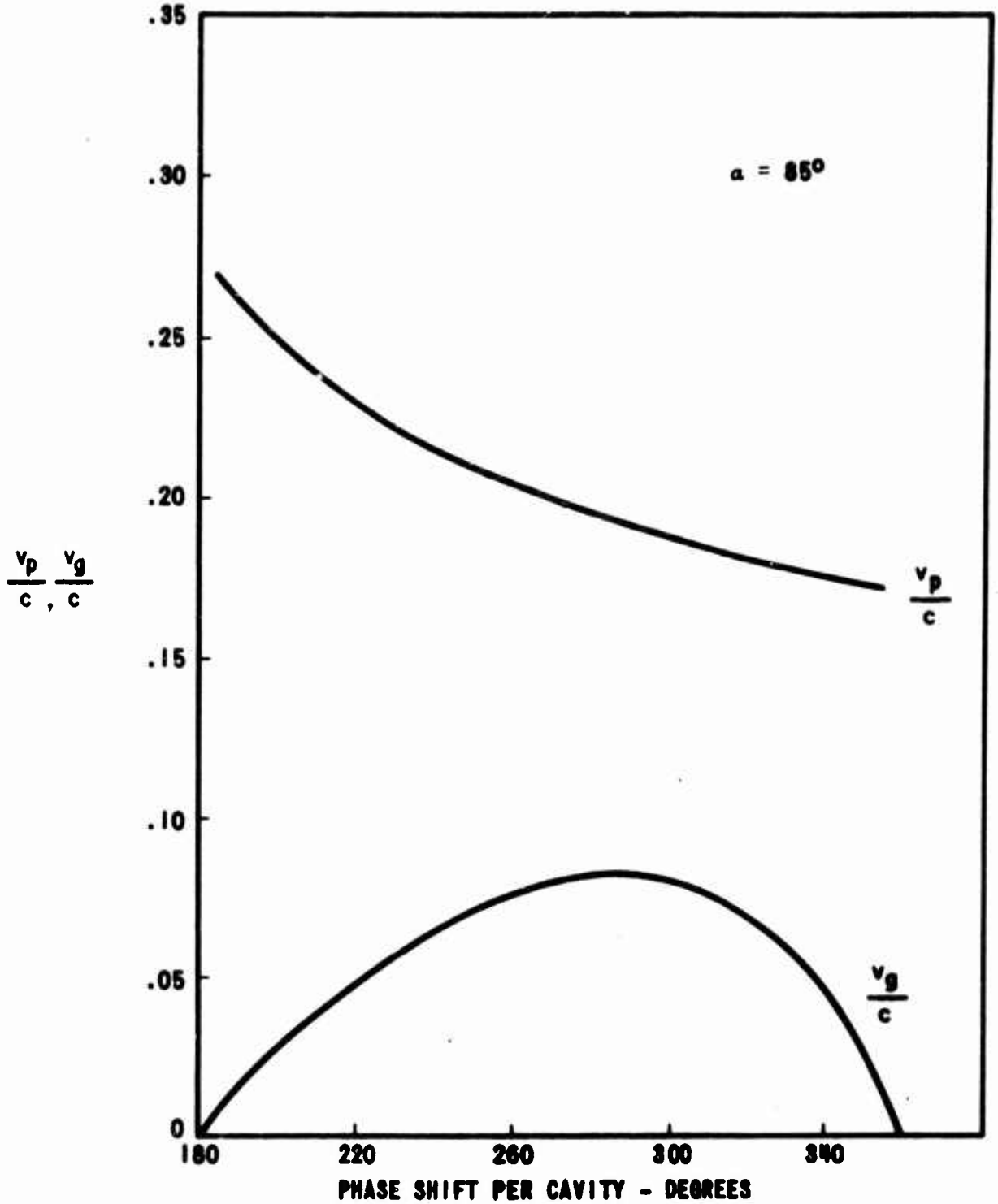

FIGURE 4-4 Phase and Group Velocities vs Phase Shift per Cavity

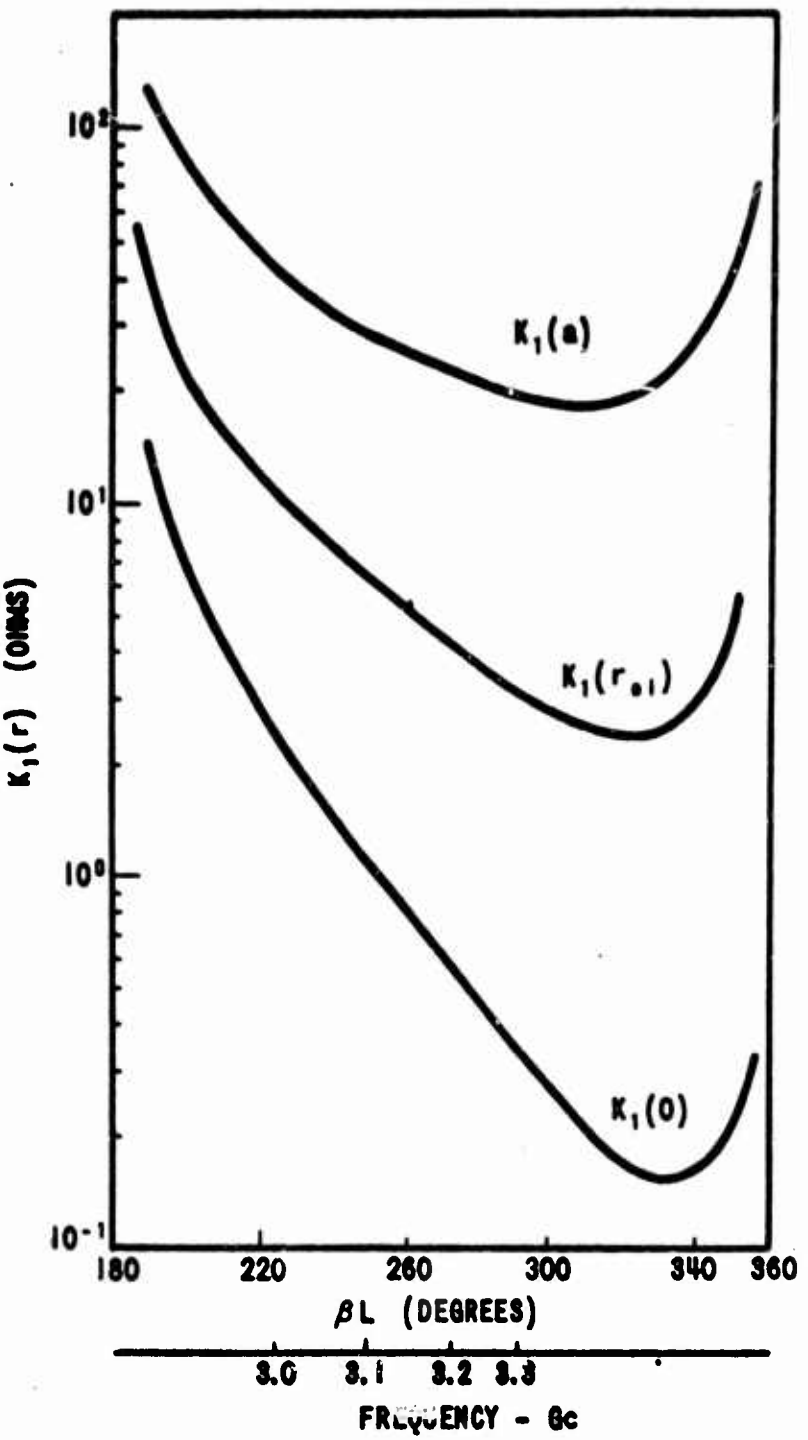

FIGURE 4-5 QR1242 Coupling Impedance

When evaluated at the beam (see Appendix B) the coupling impedance is 3.1 - 10.6 ohms. At the outset, it had been assumed that a 50 ohm coupling impedance would be achieved. Equation (1) shows that the phase shift will be $\sqrt{3/50}$, or approximately 1/4 of the expected amount. Alternatively, the rf circuit must be made four times as long to achieve the 360 degree phase shift.

The rf circuit was matched to WR284 (1.5 x 3.0 inch) waveguide. A maximum VSWR of 1.5:1 was measured on the cold test model in the 3.0 to 3.3 GHz frequency range. A matching cavity was inserted between the coupled cavity and waveguide. Drift tube gap and inductive irises have been used in the matching cavity to optimize the transition from coupled cavity to 0.360 inch height waveguide. A three-step, quarter-wave transformer increased impedance up to that of the full height waveguide. In the actual phase shifter, further adjustment of drift tube gap was required to optimize the match. VSWR was < 2 over the lower 85% of the frequency range.

The rf insertion loss was less than 2 db at 3.15 - 3.24 GHz, dropping to a minimum value of 1.2 db. Increased insertion loss at the band edges is attributable both to reduction in circuit group velocity near circuit high and low frequency cutoffs and to rf mismatch, especially in the circuit output.

5.0 DESIGN REVIEW

After coupling impedance measurements were completed, it became apparent that the coupling impedance, as averaged across the electron beam, was 3.1 - 10.6 ohms compared with the 50 ohm value estimated in the initial design. Equation (1) showed that phase shift is proportional to the square root of coupling impedance. We therefore expect a factor of 2.2 to 4.0 reduction in phase shift or alternately, a requirement that circuit length be increased by this factor to obtain the same phase shift goal. Alternative methods of approach were investigated to see if an effective gain in coupling impedance at an equivalent circuit length were feasible.

An analysis was carried out in which PPM focusing was to be applied to the folded waveguide type rf circuit. Utilizing the coupling impedance measurements made earlier, it was possible to scale impedance with circuit γa with reasonable confidence. Unfortunately, this results in an even longer tube than the earlier approach. The reason for this is that the rf circuit design requires operation at $\beta L = 3\pi/2$ while the magnetic field design requires operation at a ratio of plasma wavelength to period of over 2, for a reasonable level of beam ripple (e.g. 5%). These two constraints coupled with the requirement that peak field be below the coercive force of some of the higher coercive force magnetic materials (oriented ferrites were used), were computed and the results shown in Figures 5-1 through 5-4. The significant quantities plotted on the abcissa are $\lambda p/L$ (which must be over 2 for beam transmission considerations); rf circuit length, and Brillouin value of magnetic field which should be maintained at or below 1200 gauss as a first approximation to what can be generated. The figures show that no matter how we adjust γr_1, γa and r/a, while staying within the limits imposed by $\lambda p/L$ and B_b, the rf circuit length is well over the 80" circuit length we started with. The conclusion is that the combination of constraints forces too low a phase shift per unit length of rf structure.

To obtain a higher coupling impedance than achieved earlier in this program with a folded waveguide structure, we may consider use of a ring-bar structure, since this latter circuit will have adequate bandwidth, coupling

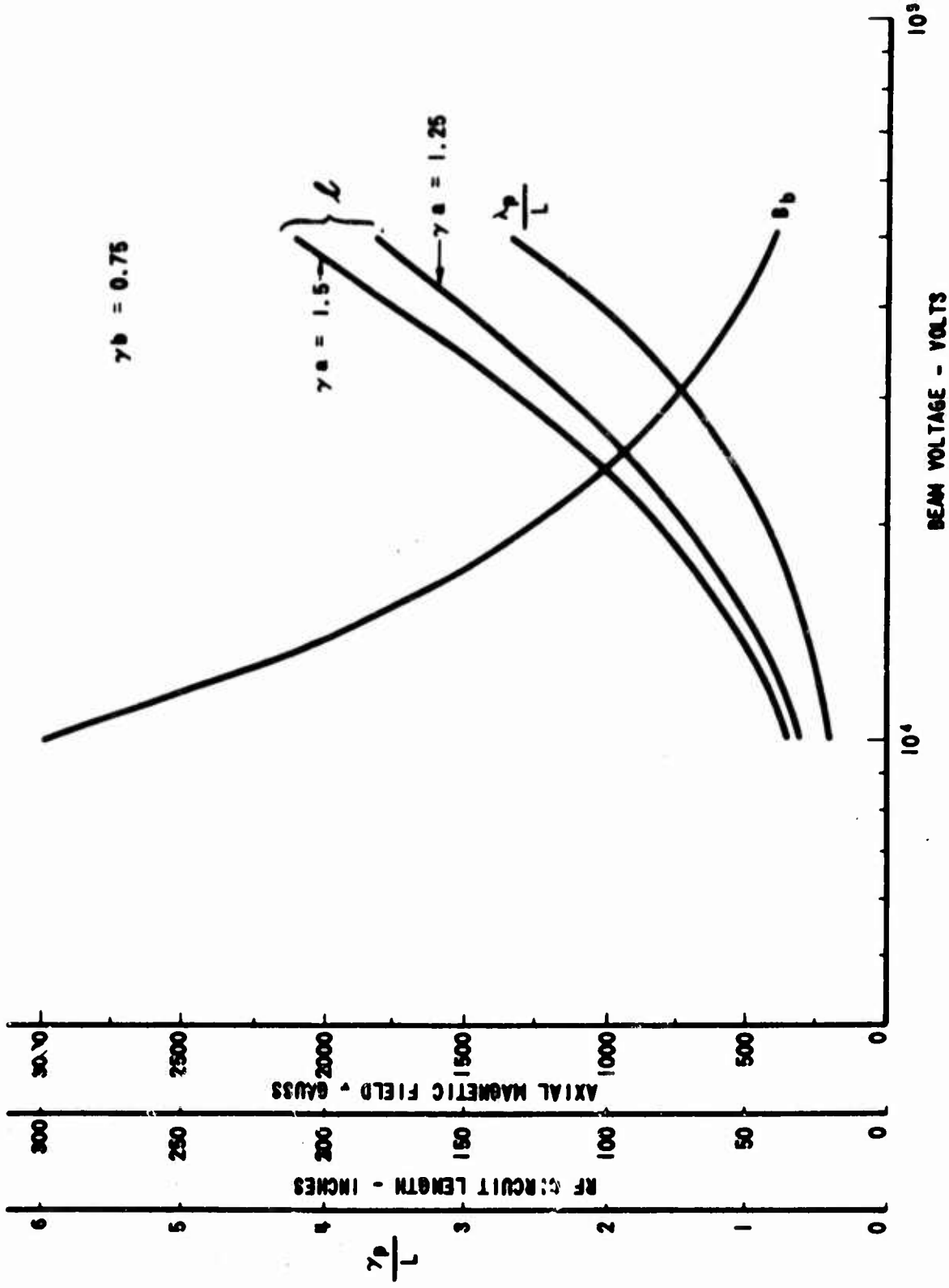

FIGURE 5-1 $\frac{\lambda_p}{L}$, RF Circuit Length, and B_z vs V_o
(γ_b = 0.75)

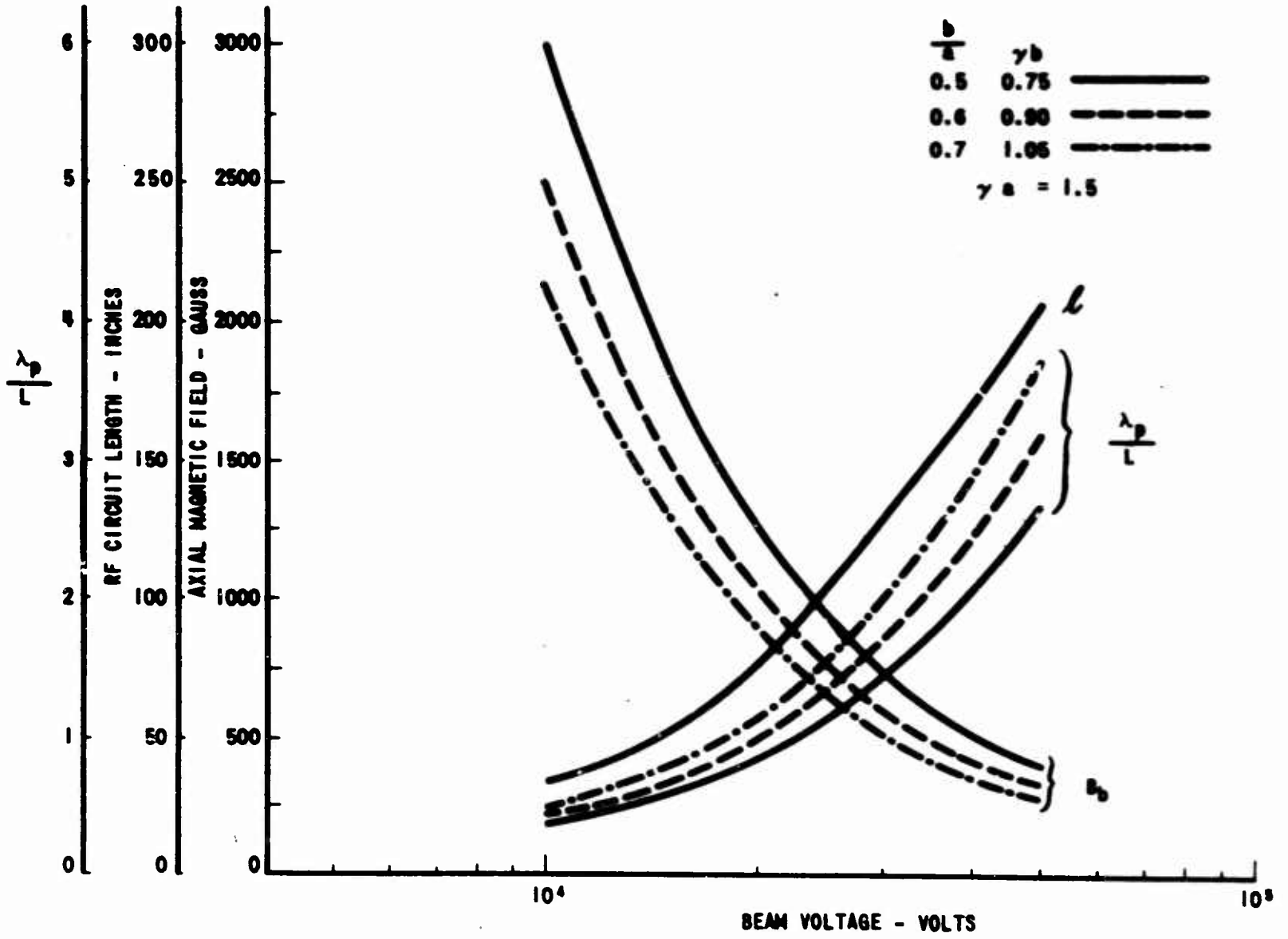

FIGURE 5-2 $\frac{\lambda p}{L}$, RF Circuit Length, and B_z vs V_o

(γa = 1.5)

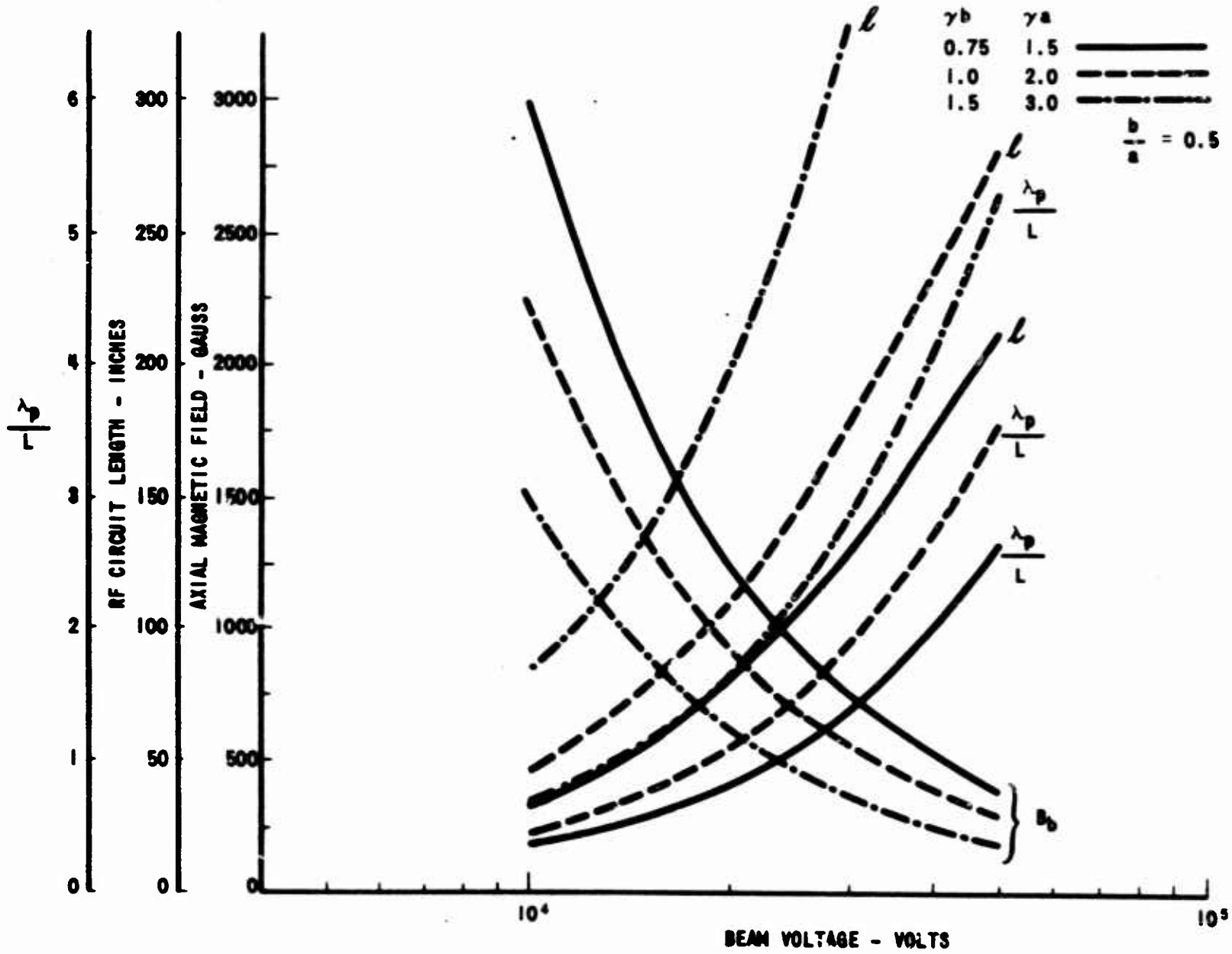

FIGURE 5-3 $\frac{\lambda_p}{L}$, RF Circuit Length, and B_z vs V_o $(\frac{b}{a} = 0.5)$

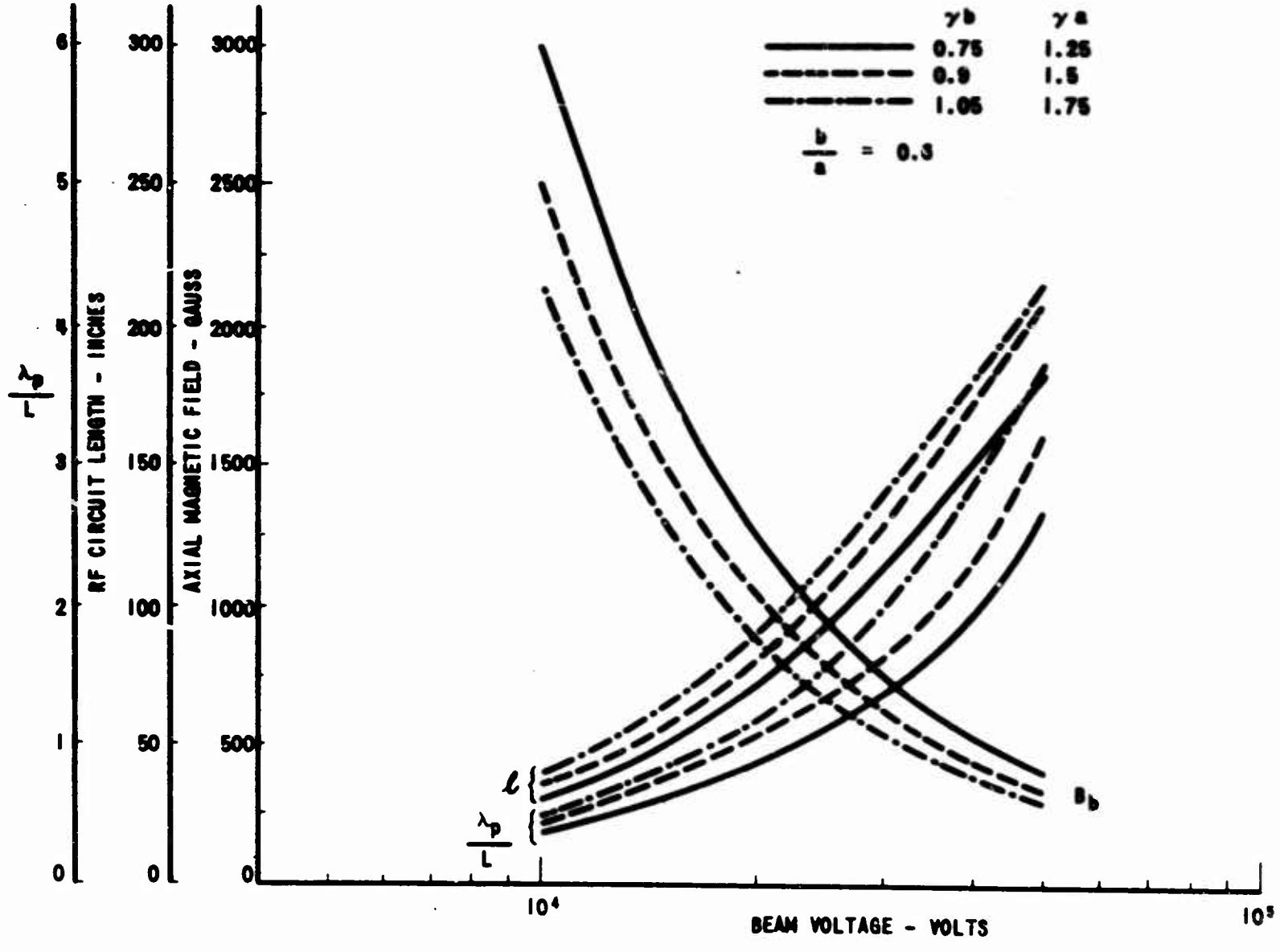

FIGURE 5-4 $\frac{\lambda_p}{L}$, RF Circuit Length, and B_z vs V_o

$(\frac{b}{a} = 0.6)$

impedance almost twice as high as a unifilar helix, but insertion loss comparable with a helix. To obtain an experimental benchmark, QR1242 #2, a ring-bar phase shifter, was measured for rf match and insertion loss. The insertion loss was 0.1 db/inch at 1000 MHz. Therefore, we see that 20 - 30 inches of this contrawound helix would have 2 - 3 db insertion loss. Scaling this structure up in frequency by a factor of 3 would result in further insertion loss.

If deviations in magnetic focusing were to be considered, it appeared that a good direction would be to maintain use of a thin hollow beam, thus achieving a high value of C and therefore high phase shift per unit length. A solid beam would not allow achievement of as high a gun perveance and therefore not as high as C. Utilizing an available magnetron injection gun, and scaled versions therefore, and a ring-bar slow wave structure, operating at 10 kv shows that a magnetic field of 1200 and 1940 gauss would result in rf structures of 30 and 19 inch lengths respectively. Producing these levels of magnetic field over the indicated lengths would result in a rather large focusing structure.

A parallel effort was conducted to carry the theoretical study of the phase shifter to a higher level of understanding. This work was carried out and is described in detail in Appendix C of this report.

At this point, it was determined that the best experimental approach would be to continue with the original structure while holding the rf circuit length below 2 feet long, thereby preventing the construction of what might have been a prohibitively large device.

6.0 MECHANICAL DESIGN

6.1 Over-all Concept

The phase shifter is constructed entirely of metal and ceramic. Wherever possible, available parts and/or subassemblies have been incorporated into the design. This breadboard model is based on electric design principles directed towards minimum size and weight. However, whenever discretion indicated, excess weight may have been added to assure adequate mechanical strength.

Major subassemblies are of brazed construction and designed to allow inspection. Final assembly uses heliarc welding. No assembly containing the cathode is furnace brazed so that the cathode is never exposed to high temperatures until bakeout on the pump.

A one liter VacIon pump is incorporated as a vacuum appendage pump to allow pumping of any gas which might be liberated during initial phase shifter operation.

The assembled phase shifter is 36 5/8 inches long and fits into a seven inch ID solenoid.

6.2 Electron Gun

The cathode is an active nickel sprayed with a triple carbonate coating. The heater is serpentine formed tungsten wire which is trapped between two ceramics. This standard Raytheon design results in a rugged heater with some thermal conduction between heater and cathode. The cathode-heater subassembly is supported by four tabs made of Hastalloy B, a low thermal conductivity material with high strength at elevated temperatures. The resultant heater-cathode subassembly is efficient thermally, and mechanically rugged.

The grid uses gold plated molybdenum mesh (0.017 inch diameter wires with 0.020 inch pitch) which is brazed to a copper grid support ring. This ring provides both a heat sink for the mesh and a welding lip to join the grid with the cathode subassembly. Jigging slots are placed in the outer sleeve to allow precise control of cathode to grid spacing during assembly. This subassembly is jigged with respect to the anode support ring and welded in place.

The anode is a 0.015 inch thick molybdenum disc which has been photo-etched to the proper geometry. The anode is brazed to a copper ring which results in a good thermal conduction cooling path for the anode. The anode and anode ring are welded into the anode support ring.

By careful jigging and machining operations, spacings and concentricity between cathode, focus electrode, grid, anode, and gun welding flange are assured.

6.3 Rf Circuit

The coupled cavity structure is fabricated out of 38 identical copper laminations. The laminations are so designed that a 180° rotation of successive laminations produces the coupled cavity structure. The laminations are silver plated at the surfaces of contact when stacked. Alignment pins are used to position the laminations during assembly and to strengthen the coupled cavity circuit. The 38-lamination coupled-cavity structure, and the similarly silver-plated input and output matching cavities are brazed as three separate subassemblies at 850°C. After inspection, these three subassemblies are brazed at 825°C into the total coupled cavity circuit subassembly.

The input and output waveguides are made of OFHC copper with cupronickel brazing straps. Copper transformer blocks are heliarc welded into the waveguide. Welding flanges are eutectic silver-copper brazed to both ends of the waveguides.

The window assembly contains the ceramic vacuum window in a poker chip in circular waveguide design, a welding flange on one side and waveguide flange on the other side.

The coupled cavity, waveguide, and window subassemblies are welded together. Bracing straps and mounting blocks are welded on at this time to assure a rugged structure.

6.4 Collector

The collector is a piece of copper tubing with molybdenum plug and post brazed on the inside. The center post is inserted to raise the potential within the electron beam and thereby improve collector depression capability. The post is made of molybdenum to provide mechanical strength at the potentially high operating temperatures. A ceramic insulator bushing is used to allow depressed collector operation.

7.0 TEST SETUP

The rf test setup is shown, in block diagram form, in Figure 7-1. A phase bridge is formed such that the QR1242 phase length is compared with that of a fixed length of coaxial cable. This is done by splitting the drive signal in a 30 db directional coupler. Part of the drive signal passes through the phase shifter and is then coupled to the slotted line creating a wave moving from right to left in the slotted line of Figure 7-1. A sample of the drive signal is coupled out, passes through a delay line setting up a wave moving from left to right in the slotted line. A standing wave pattern is set up in the slotted line, with the phase of the standing wave pattern dependent upon the relative lengths of the two arms of the bridge.

The standing wave pattern is sampled with a pair of probes with fixed relative spacing. When the probes exactly straddle the standing wave pattern minimum, a null is observed on the oscilloscope. As the null is tracked in position, a sensitive indication of differential phase shift is achieved.

The delay line is a length of coaxial cable which is so made that the two arms of the phase bridge are approximately equal. If the two arms were exactly the same electrical length, and all components frequency insensitive, a standing wave minimum would be found which did not move as frequency is changed. Alternatively, with equal length arms, changes in frequency, within the rf pulse or from pulse to pulse, introduce negligible error because of differential phase changes in the bridge components. Since the phase length of the phase shifter is a function of frequency, only its sensitivity dictates the frequency stability requirements for the drive signal source.

The attenuators on each side of the slotted line are inserted to reduce the VSWR as seen looking out from either end of the slotted line. These attenuators are inserted to reduce rapid variations in phase with frequency due to long line effects.

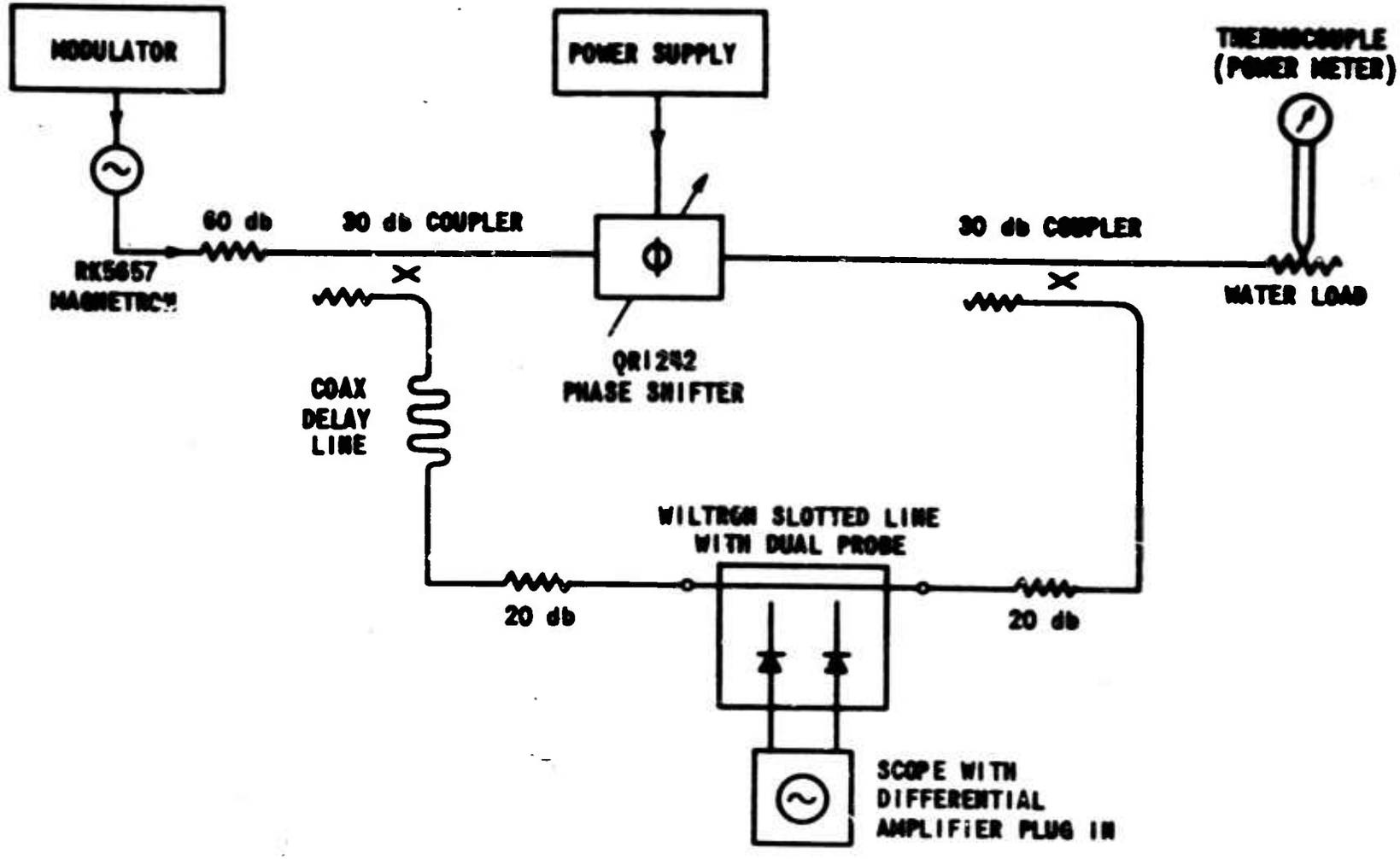

FIGURE 7-1 Block Diagram of RF Test Setup

The RK5657 is capable of an 800 kw peak power output. The 6 db attenuator is inserted to reduce this drive signal to the QR1242 to a maximum of 200 kw. Reduction of RK5657 anode current is used to drop the drive power to lower levels.

QR1242 power output is monitored by a water load. Since insertion loss of the directional couplers, 6 db pad, and QR1242 have been previously measured, QR1242 input power can be determined at QR1242 current cut off.

Frequency has been measured by breaking the bridge and using a wavemeter.

The QR1242 power supply is set up with a dc voltage applied from cathode to ground. Anode, rf circuit, and collector are all operated at ground potential. A 0-300 volt dc power supply biases the grid to cutoff. A pulse is superimposed on the cathode-to-grid bias, pulsing the beam on.

Collector depression capability can be tested for by biasing the collector negative with respect to ground, all other voltages being maintained as described.

Peak collector and rf circuit currents are monitored by calibrated viewing resistors. Peak cathode current is measured by means of a transformer which encircles the cathode lead. All other pertinent currents and voltages are monitored by metering the power supply console.

8.0 TEST RESULTS

Complete test data were not taken because of emission limitations of the cathode which became worse with time. Data showed that the phase shifter did have a beam voltage at which maximum phase shift occurred, as theoretically predicted in Figure 7-3 of Appendix C, and experimentally observed on an S-band phase shifter shown in Figure 7-5 of Appendix C. In the QR1242, optimum phase shift occurred at 11 KV. A measurement at f = 3.127 GHz, 100 kw, and 0.00106 duty resulted in a 4.28° of phase shift, where equation (1) predicts 2.94°. This level of phase shift is directly attributable to the low cathode current and, in fact, shows good agreement with the theory that, with full current, 118 degrees of phase shift would have been theoretically achieved at this frequency.

9.0 MANPOWER LEVEL

The level of effort expended during this program is shown in Table 9-1. The discrepancy between the projected manhours determined prior to program start and actual manhours reflects an increased percentage of engineering effort expended in attempting to determine alternative design approaches to achieve the design goals.

TABLE 9-1.
QR1242 MAN HOUR SUMMARY

Description	Projected (hr)	Actual (hr)
Assembly	800	1667
Exhaust	100	23
Cold Test		4
Hot Test	400	47
Engineering	1730	2074
Machine Shop	800	295
Drafting	500	87
Technical Writing		93
Cathode Manufacture	84	6
Materials and Techniques	127	30
Instrumentation	170	133
Quality Assurance		32
TOTAL	4711	4491

10.0 SUMMARY

A program directed towards the design and development of a breadboard model of a 100 kw S-band electron beam phase shifter has been carried out. A phase shifter was designed and built, but test data limited due to an emission limited cathode. A single data test point showed good agreement with the predicted theoretical phase shift. Operation at rf drive of 100 kw and 0.001 duty was demonstrated. The rf insertion loss for this long rf circuit was 1.2 db at midband. To keep the phase shifter to its 36 5/8" length the slow-wave circuit was chosen to be consistent with a predicted 112° phase shift. The electron beam phase shifter, has been analyzed in terms of phase shift, harmonics, and other non-linear phenomena.

11.0 REFERENCES

1. Final Report, "QK1242 Research Program, The Electron Beam Phase Shifter", Raytheon Company, Microwave and Power Tube Division, RADC Contract No. AF30(602)-3161, June 20, 1963 to August 31, 1964.

2. Winsor, D. L. and Yacus, J., "An Electronic Microwave Phase Shifter," Proceedings of Symposium on Electronically Scanned Array Techniques and Applications, July 1964, pp 173-87.

3. Pierce, J. R., "Traveling-Wave Tubes," D. Van Nostrand Company, Inc. 1950, p. 17, equation (2.43).

4. Dunn, D. A., "Traveling-Wave Amplifiers and Backward-Wave Oscillators for VHF," IRE Trans, ED, July 1957, pp 246-64, equation (39).

5. Spangenberg, K. R., "Vacuum Tubes," McGraw-Hill Book Company, Inc., 1948, Chapters 7 and 8.

6. Wolkstein, H. J., "Design Considerations for Grid-Controlled Electron Guns for Pulsed Traveling-Wave Tubes," RCA Review, September 1960, pp. 389-413.

7. Nalos, Proc. IRE October 1954, p 1509.

8. Lagerstrom, R. P., "Interaction Impedance Measurements by Perturbation of Traveling Waves," Technical Report No. 7, Stanford Electronics Laboratories, Feb. 11, 1957.

APPENDIX A

ROME AIR DEVELOPMENT CENTER
GRIFFISS AIR FORCE BASE
NEW YORK

12 August 1964

Purchase Request Continuation Sheet

For: High Power S-Band Electron Beam Phase Shifter Techniques

Continuation Sheet No. 1 For P. R. No. 65-209

DESCRIPTION OF SUPPLIES OR SERVICES TO BE PURCHASED

ITEM	QUANTITY	DESCRIPTION
1		DESIGN AND DEVELOPMENT of a breadboard model (as defined in Note 1) of a high power S-band Electron beam Phase Shifter. The information obtained under Contract AF30(602)-3161 shall be used as a starting point. This phase shifter shall have the following design objectives:

a. Operating Frequency Range - 3000-3300 megahertz (MHz)

b. Peak Power - 100 kilowatts (kw)

c. Average Power - 100 watts

d. Low Level Insertion Loss - Max 0.5 decibel (db)

e. Electronic Phase Control - 360°

f. The phase control power shall be a minimum 1/5 of the microwave power.

g. Focusing Structure - Permanent Magnet

h. The voltage standing wave ratio of the helix structure with couplers shall not exceed 1.3.

THE INFORMATION CONTAINED HEREIN SHALL NOT BE RELEASED TO UNAUTHORIZED PERSONS PRIOR TO RELEASE OF THE INVITATION FOR BIDS (IFB) OR REQUEST FOR PROPOSAL (RFP), AFPI 1-465 (d) (1)

i. Accuracy - The phase shifter shall have an absolute accuracy of plus or minus 3 degrees of phase shift.

j. The phase shift in degrees shall be a linear function of the beam current.

k. Phase control power supply with appropriate and accurate indicating meters shall be included.

l. The phase shifter shall be designed for minimum weight, size and power consumption commensurate with optimum electrical performance.

ENGINEERING SERVICES to investigate the following:

a. The contributions and effects of noise to the performance of the phase shifter.

b. The generation and effects of spurious and harmonic frequency contributions to the performance of the phase shifter:

Data shall be delivered as documented on the attached DD Form 1423 entitled: "Contractor Data Requirements List". The essential data requirements are as follows:

1. CONTRACT STATUS REPORT shall be prepared in letter form and shall include at least the following:

   a. A summary of the work performed during the reporting period.

   b. Conformance or nonconformance to projected work schedule

   c. An analysis of work progress covering the reporting period.

   d. A short statement of work effort planned for the next reporting period.

   e. A statement describing significant changes in the contractors operating personnel.

2. TECHNICAL DOCUMENTARY REPORT shall be provided to record the technical efforts and achievements under Items 1 and 2. Each TDR shall be prepared in accordance with the requirements of Chapter 2 of AFSCM 5-1 entitled: "Technical Documentary Reports", dated 1 November 1961 and Interim Change 1 to AFSCM 5-1 dated 31 July 1963 except for the following:

   a. Reproduction shall not be considered a function of the contractor so references to printing shall not apply except as to intent.

   b. The only copy submitted shall be the "draft copy" (and carbons).

   c. The "draft copy" shall be an "edited" draft suitable for typesetting and printing with a minimum of review on the part of the procuring activity. Art and linework shall be in final form.

   d. Disregard the references to the AFSC document number or leave a space as applicable.

   Note 1 - Breadboard Model - An assembly of preliminary circuits and parts to prove the feasibility of a device, circuit, or principle in its simplest possible form.

APPENDIX B

Gap Factor for Thick Beams

The gap factor is a means of correcting coupling impedance for transit time and radial field variation. Pierce shows* that in the case of a uniform axial field acting on a nongridded gap the electric field is modified by the gap factor:

$$M = \left[\frac{\sin(\beta\ell/2)}{(\beta\ell/2)}\right]\left[\frac{I_o(\gamma r)}{I_o(\gamma a)}\right] = M_\ell M_r \qquad \text{(B-1)}$$

The interaction impedance, K, is proportional to the square of the electric field, and therefore proportional to M^2. The coupling impedance is tc be evaluated over that portion of the gap which is intercepted by the electron beam. The mean squared value of the radial portion of the gap factor is given by**

$$M_r^2 = \frac{1}{A_b}\int_{r_i}^{r_o} \frac{I_o^2(\gamma p)\, 2\pi\rho\, d\rho}{I_o^2(\gamma a)} \qquad \text{(B-2)}$$

where A_b is beam area for a beam of inner and outer radii r_i and r_o, respectively.

A solid beam of radius b ($r_o = b$, $r_i = 0$) has

$$M_{r\,\text{solid}}^2 = \frac{I_o^2(\gamma b) - I_1^2(\gamma b)}{I_o^2(\gamma a)} \qquad \text{(B-3)}$$

---

* Pierce, J. R., "Traveling-Wave Tubes," D. Van Nostrand Company, Inc., 1950, p. 17, equation (2-43).

** Puts, J. L., and Luebke, W. R., "A High Power S-Band Backward Wave Oscillator," Technical Report No. 182-1, Stanford University, Feb. 24, 1956.

In a hollow thin electron beam of radius b ($b = r_o \approx r_i >> r_o - r_i$) we find

$$M^2_{r_{thin}} = \frac{I_o^{\,2}(\gamma b)}{I_o^{\,2}(\gamma a)} \tag{B-4}$$

Equation (B-4) properly fits the evaluation of coupling impedance at a given radial position. In the case of a thick hollow beam, ($r_o = b$, $r_i = c$) we obtain:

$$M^2_{r_{thick}} = \frac{(\gamma b)^2 \left[I_o^{\,2}(\gamma b) - I_1^{\,2}(\gamma b)\right] - (\gamma c)^2 \left[I_o^{\,2}(\gamma c) - I_i^{\,2}(\gamma c)\right]}{\left[(\gamma b)^2 - (\gamma c)^2\right] \quad I_o^{\,2}(\gamma a)} \tag{B-5}$$

Equation (B-5) reduces to the solution for solid and thin hollow beams when $c = 0$ or when $b = c$ respectively.

RAYTHEON COMPANY
Microwave and Power Tube Division
Waltham, Massachusetts

APPENDIX C

THE THEORY OF OPERATION OF THE ELECTRON BEAM PHASE SHIFTER

by

W. R. Curtice

Approved: L. L. Clampitt

L. L. Clampitt, Manager of Engineering,
Microwave Tube Operation

PT-1019
January 20, 1966

ABSTRACT

The electron beam phase shifter is analyzed by calculating the ballistic electron bunching produced by the circuit electric field and then finding the voltage induced in the circuit by the fundamental frequency component of electron current. The method of successive approximation of the electric field solution is shown to yield an accurate design equation for phase shifters. One solution is obtain by computer calculations of electron trajectories and several analytical solutions are developed which are valid only for reasonably short devices.

The computer calculated solution is used to produce an accurate solution for operation with the beam velocity slightly less than the circuit wave velocity and this solution is seen to produce nearly maximum phase shift with small circuit amplitude change. The effects of electron space charge and beam synchronism are discussed. Calculations are given for the early test vehicles and the agreement is found to be good. The empirical design relation previously developed in earlier studies is verified. Finally, harmonic output power and other non-linear phenomena are discussed.

TABLE OF CONTENTS

LIST OF ILLUSTRATIONS

1.0 INTRODUCTION

The linear-beam phase shifter was conceived at Raytheon Company[1] as a new element for phase control in phase array radar systems. It was envisioned as a device utilizing a broadband traveling-wave circuit whose phase characteristic could be varied by use of a low power linear beam. Such a device will have continuously variable phase control and the capability of phase changes in nanoseconds. Early devices did, in fact, provide phase control at high power levels with low insertion loss, although their design was not understood very well. It has since been possible to explain the operation of these devices with both a simple first-order design equation and a more elaborate theory which predicts both amplitude and phase changes through computer calculation of the large signal beam and circuit interaction. The calculated phase characteristics are in good agreement with measurements whereas no amplitude measurements are available for comparison.

Figure 1-1 illustrates the electron beam phase shifter. The device consists simply of a section of slow-wave structure without attenuation, an electron gun with a current control electrode, and a collector. Careful experiments to measure the change produced in phase shift as beam voltage and current were varied for an rf drive power level of one-half to five times the beam power showed the following characteristics (for experimental data, see Reference 1):

1. Maximum phase increase always occurred at a beam voltage near the voltage corresponding to beam and circuit wave synchronism.
2. No significant phase control was measured when the beam and circuit power flow were in opposite directions.
3. The phase increase was very nearly a linear function of the beam current value.
4. Maximum phase shift occurred with low increased insertion loss (typically less than 1 db).
5. The maximum phase shift varied inversely as the square root of the rf drive power for a fixed beam power.
6. Neither the polarity nor the magnitude of the magnetic focusing field had a strong effect upon the phase change.

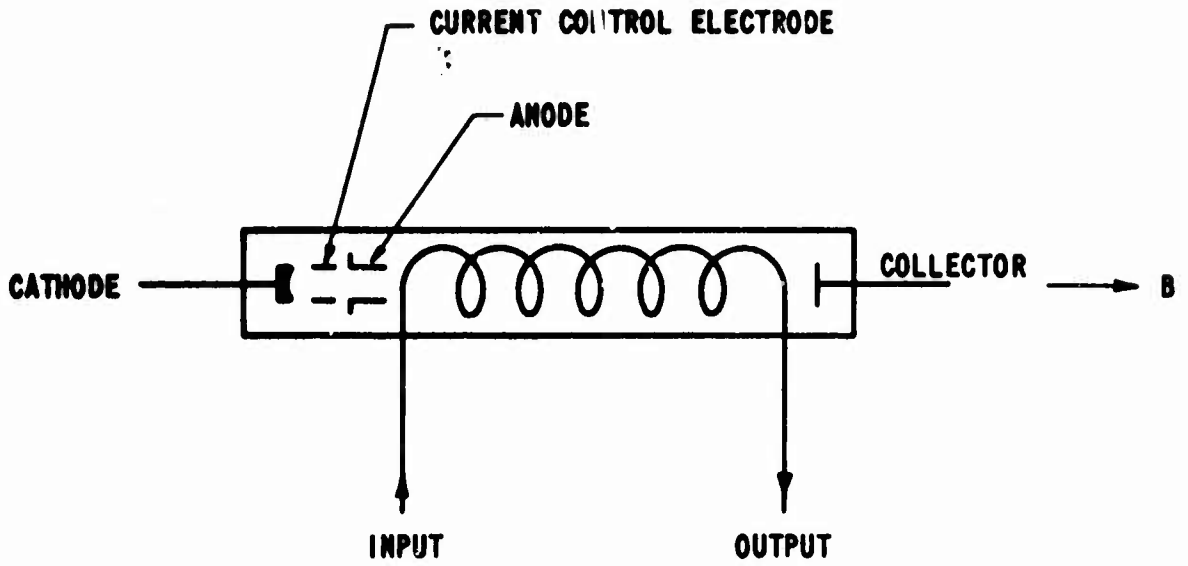

FIGURE 1-1 The Electron Beam Phase Shifter

7. One test vehicle consisted of two operable and separate helix sections. The phase shift was doubled by using both sections in series, and the phase shift was independent of cable length between the two sections.

An analysis of operation was sought that would reasonably explain these observations and provide criteria for design purposes. The obvious dependence upon some synchronism condition suggests that a suitable theory of operation should be obtainable through the analysis of the large signal bunching of the electron beam by the circuit fields. Significant ac current should result early in the device. By assuming that this ac current persists at some saturation level throughout the remainder of the device, a derivation was made based upon the perturbation of the usual field equation of the slow-wave structure. This derivation resulted in an expression for phase change which agreed with the experimental observations. The analysis presented herein verifies that this assumption and solution is valid to a first approximation and furthermore presents a more accurate method for calculation of phase and amplitude changes in such a device.

2.0 ASSUMPTIONS FOR THEORETICAL DERIVATION

Several restrictive assumptions are made to simplify the analysis. All are consistent with the experimental observations. The fundamental assumption utilized here is that the electron beam influences the slow-wave circuit fields only as a perturbation. That is, the circuit field change (produced by the electron beam) per unit length of the circuit is small (Typically the phase increase observed divided by the total circuit phase length is one to six percent and the total increased insertion loss is less than 1 db). Thus a crude approximation to the circuit field is the "cold" circuit field, that is, the field present when the beam is absent. The next approximation is then the cold field with a small phase lag in time and so on. The true solution for the circuit fields will show a more complicated phase and amplitude function of beam current.

Electron bunching at beam and circuit synchronism will occur due to the strong circuit electric field. The bunching results in a fundamental component of ac current which will induce a small voltage into the circuit. This voltage is approximately 90° phase lagging the original circuit voltage (i. e. the cold field) and the actual circuit electric field is then the vector sum of the original voltage plus the induced voltage. The actual circuit field therefore lags the cold circuit field and a phase shift has been produced.

The preliminary analysis will assume synchronism. That is, the electron dc velocity and the forward circuit-wave velocity are assumed equal. The non-synchronous case will be discussed later. The electron bunching will be considered from a ballistic point of view and the effect of electron space neglected until later in this report. This procedure has several advantages. First, the equations of interaction are greatly simplified. Second, and probably most important, the ballistic analysis handles electron overtaking with no difficulty (See the discussion by D. R. Hamilton[2]). This is important because overtaking will occur early in such a device.

The experimental observations concerning the magnetic focusing fields show that the device does not depend upon transverse phenomena (such as cyclotron waves) for its basic operation. Therefore, a one dimensional problem is considered and minor corrections are made for finite beam size effects as in the usual analysis of a TWT. Electrons are then assumed to be confined by an infinite magnetic field which will not allow transverse motion. Likewise, other focusing effects such as velocity differences due to space-charge depression of potential and beam interception effects due to large signals are not considered. Relativistic effects are neglected since no tubes are envisioned that require large beam voltages.

3.0 THE DERIVATION OF EQUATIONS

The equation of motion for each electron is simply

$$m_e \frac{d^2 z}{dt^2} = - |e| E_z (z, t) \qquad (1)$$

where m_e = electron mass

z = distance from the beginning of the slow-wave structure

t = time

$|e|$ = absolute value of electron space charge

$E_z(z, t)$ = the longitudinal circuit electric field present at each electron.

Defining u_o as the average electron velocity, we find that the initial velocity condition for Equation (1) is simply $\frac{dz}{dt} = u_o$ at $z = 0$. But because the electric field is assumed to be a sinusoidal time function, the entrance time for each electron must also be specified to compute this trajectory.

Because the actual electric field is dependent upon circuit voltage induced by the fundamental component of rf current, Equation (1) requires that the solution for $E_z(z,t)$ be known before deriving the electron motion. The method of successive approximation will be used to develop the actual solution for $E_z(z,t)$. The zeroth approximation for the electron field is the cold circuit field. A solution for ac beam current and induced circuit voltage can be obtained using the cold field. The solution will show that electric field is not much different than the cold field and the principle difference will be a phase lag. This solution may then be used in Equation (1) to derive a more accurate solution, and so on, until the solution obtained converges to the actual solution. Because the trial solutions are not very different, it has been found that accurate solutions are obtained on either the first or second trial.

The circuit field is assumed to be

$$E_z(z, t) = -E_o \sin(\omega t - \beta_o z), \qquad (2)$$

where E_o = the fundamental space-harmonic electric-field component for the "cold" slow wave structure which is assumed to be real for convenience.

ω = the angular frequency of the rf drive power

β_o = the fundamental space-harmonic propagation constant of the cold circuit.

It is convenient to define simpler variables as

$$T \equiv \omega t$$

$$Z \equiv \beta_o z$$

and in addition let

$$c \equiv \frac{|e| \beta_o E_o}{m_e \omega^2} .$$

Equation (1) can then be seen to give the equation of motion as

$$\frac{d^2 Z}{dT^2} = c \sin (T - Z). \tag{3}$$

Defining the starting time of each electron as t_s, the starting phase is then ωt_s or T_s. The initial conditions for Equation (3) are then

$$\left.\frac{dZ}{dT}\right|_{\substack{Z = 0 \\ T = T_s}} = 1. \tag{4}$$

Equation (3) with initial condition (4) can be solved by various means for $Z(T, T_s)$. It is found that for values of c typically encountered (such as $c = 0.10$), no electrons turn around. Thus for each T_s, Z is a single valued function of T and likewise T is a single valued function of Z. The function $T(Z, T_s)$ can then be obtained from $Z(T, T_s)$ and will be used to compute the rf current.

The beam current* is periodic and given by D. R. Hamilton[2] as

$$i = -\sum_{\substack{m = 0, \pm 1, \pm 2, \ldots}}^{\pm \infty} \frac{I_m}{2} e^{jm (T - Z)} \tag{5}$$

* Current is taken as conventional current rather than electron current to maintain consistency with the equations of field theory.

where $I_m = \frac{I_o}{\pi} \int_{-\pi}^{\pi} e^{-jm(T-Z)} \, dT_s$ (6)

and $I_{-m} = I_m^*$ (7)

since the current is real $(j = \sqrt{-1})$.

Equation (6) with $T(Z, T_s)$ allows calculation of I_1 and I_{-1}.

The equation for the interaction of a forward-wave circuit and the fundamental ac beam current for a circuit wave of form exp j $\{\omega t - \beta z\}$ is[3]

$$\frac{d^2 E_z(z)}{dz^2} + \beta_o^2 E_z(z) = j \beta_o \beta^2 K_c i_z(z) \quad (8)$$

where β = actual "hot" propagation constant for the circuit

K_c = Pierce's coupling impedance[4] $= \frac{E_o^2}{2\beta^2 P_{rf}}$

P_{rf} = rf drive power

$i_z(z)$ = the fundamental frequency component of ac beam current.

Since only a small change in β is observed, little accuracy will be lost by setting $\beta = \beta_o$ on the right hand side of Equation (8) for the first trial solution. Then using the variable Z, Equation (8) becomes

$$\frac{d^2 E_z(Z)}{dZ^2} + E_z(Z) = j \beta_o K_c i_z(Z) \quad (9)$$

The ac beam current by Equation (5) is

$$i_z(Z, T) = -\frac{I_1}{2} e^{j(T-Z)} - \frac{I_1^*}{2} e^{-j(T-Z)} . \quad (10)$$

Expression (2) for the cold circuit field can be written as

$$E_z(Z,T) = \frac{jE_o}{Z} e^{j(T-Z)} - \frac{jE_o}{Z} e^{-j(T-Z)} . \quad (11)$$

It is assumed that the actual electric field can be written as

$$E_z(Z,T) = j\frac{E_o F(Z)}{Z} e^{j(T-Z)} - j\frac{E_o F^*(Z)}{Z} e^{-j(T-Z)} , \quad (12)$$

where $F(Z)$ is a slowly varying function of Z and not very different from unity.

Substitution of the first term of expressions (10) and (12) into Equation (9) gives the equation

$$j\frac{d^2F}{dZ^2} + 2\frac{dF}{dZ} = -j\frac{\beta_o K_c I_1}{E_o} \quad (13)$$

which is also obtained by substitution of the second term in expressions (10) and (12) into the conjugate form of equation (8).

Equation (13) can be integrated once and the integration constant evaluated from the initial condition

$$F(o) = 1.0$$

$$\left.\frac{dF}{dZ}\right|_{Z=0} = 0 \quad (14)$$

The integration of Equation (13) produces the equation

$$j \frac{dF}{dZ} + 2 (F-1) = -j \frac{\beta_o K_c}{E_o} \int_o^Z I_1 \, dZ. \qquad (15)$$

The solution to Equation (15) is

$$F(Z) = 1 - \frac{\beta_o K_c}{E_o} e^{j2Z} \int_o^Z e^{-j2Z_1} \int_o^{Z_1} I_1(Z_2) \, dZ_2 \, dZ_1 \qquad (16)$$

however this expression results in quite lengthly computations. To simplify the computations, an approximation will be used. Since F(Z) is a slowly varying function of Z, $\frac{dF}{dZ}$ is small and $\frac{d^2F}{dZ^2}$ is very small. If $\frac{d^2F}{dZ^2}$ is set equal to zero in Equation (13), an approximation for the first deviation is found to be

$$\frac{dF}{dZ} \approx -j \frac{\beta_o K_c I_1}{2E_o} \qquad (17)$$

Using expression (17) in Equation (15) will give an accurate equation for the calculation of F(Z) and it is

$$F(Z) = 1 - j \frac{\beta_o K_c}{2E_o} \int_o^Z I_1 \, dZ - \frac{\beta_o K_c I_1}{4E_o} \qquad (18)$$

It can be shown that Equation (18) is an accurate solution to Equation (13) if

$$\left| \frac{1}{4} \frac{d^2}{dZ^2} \frac{I_1}{I_o} \right| << \left| \frac{I_1}{I_o} \right| . \qquad (19)$$

In subsequence by using derivations of I_1/I_o, the quantity on the left hand side will be seen to be from 10 to 100 times smaller than the quantity on the right hand side.

Using the definition of c, and the relationships

$$\frac{\omega}{\beta_o} = u_o$$

$$\frac{1}{2} m u_o^2 = |e| V_o$$

$$\frac{V_o}{I_o} = K_o$$

where V_o = dc beam voltage
I_o = dc beam current
K_o = dc beam impedance,

then it is easily shown that

$$\frac{\beta_o K_c I_o}{2 E_o} = \frac{K_c}{4c K_o} \tag{20}$$

and Equation (18) can be written as

$$F(Z) = 1 - j \frac{K_c}{4cK_o} \int_o^Z \frac{I_1}{I_o} dZ - \frac{K_c}{8c K_o} \cdot \frac{I_1}{I_o} \tag{21}$$

Equations (3), (4), (6), and (21) constitute a set of equations suitable for solution of this problem by successive approximation. For each cycle a function F(Z) will be obtained. The phase change produced by beam current is given by the angle between the vector F(Z) and the unity vector and amplitude changes are given by the magnitude of $|F(Z)| - 1$.

4.0 ANALYTICAL SOLUTIONS FOR ELECTRICALLY SHORT DEVICES

It would be extremely useful to develop an accurate analytical solution to the actual electric field in the electron beam phase shifter. However, the complexity of the problem becomes unreasonable for electrically long devices and the only analytical solutions sought will be those that apply to short slow-wave structures. The long devices will be treated later in this report through computer computation.

First a solution $Z(T, T_s)$ must be found for Equation (3). Because the equation is transcendental, a suitable method for finding an approximate solution is again the method of successive approximation. Assume that the electron motion is approximately described by its trajectory in the absence of an electric field, that is

$$Z \approx T - T_s \tag{22}$$

The right hand side of Equation (3) is then approximately $c \sin T_s$ and the solution for this equation subject to the boundary conditions (4) is

$$Z \approx (T - T_s) + \frac{c}{2} \sin T_s \, (T - T_s)^2 \tag{23}$$

Equation (23) expresses Z as the approximation (22) plus a correction term. A more accurate expression for Z is obtained by using (23) in the right hand side of Equation (3). The result is

$$Z \approx (T - T_s) + \frac{c}{2} \sin T_s \, (T - T_s)^2 - \frac{c^2 \sin 2 T_s}{4} (T - T_s)^4. \tag{24}$$

Obviously this method generates a power series expansion for Z in terms of $T - T_s$. Since c is typically 0.10 or smaller, this series will be a good approximation for some range of $T - T_s$. To calculate the ac current, the expression

$T(Z, T_s)$ must be obtained. This can be done as a series expansion. Assuming that

$$T - T_s = \sum_{n = 0,\ 1,\ \ldots}^{\infty} a_n Z^n, \tag{25}$$

and evaluating the first four terms, it can be shown that

$$T - T_s \approx Z - \frac{c \sin T_s}{2} Z^2 + \frac{c^2 \sin^2 T_s}{2} Z^3 + \left(\frac{c^3 \sin^2 T_s \cos T_s}{16} - \frac{c^3 \sin^3 T_s}{8} \right) Z^4 \tag{26}$$

Equation (26) can also be written as

$$\frac{T - T_s}{Z} \approx 1 - \frac{\sin T_s}{2} (cZ) + \frac{\sin^2 T_s}{2} (cZ)^2 + \frac{\sin^2 T_s}{16} (\cos T_s - 2 \sin T_s) (cZ)^3 \tag{27}$$

Equation (25) shows that $\frac{T - T_s}{Z}$ is really being expanded in powers of cZ and accuracy will decrease as cZ increases. Since Z represents the normalized length of slow-wave structure, the expansion will only be accurate from the beginning of the structure up to same value of Z determined by the magnitude of c. Small c allows accuracy to larger values of Z.

By Equation (6), the fundamental current component is

$$\frac{I_1}{I_o} = \frac{1}{\pi} \int_{-\pi}^{\pi} e^{-j(T - Z)} \, dT_s \tag{28}$$

Using the definitions

$$X \equiv \frac{cZ^2}{2}$$

$$Y = \frac{c^2 Z^3}{4} \tag{29}$$

and employing only the first three terms in expansion (26), the integral (28) can be shown to be

$$\frac{I_1}{I_o} \approx e^{-jY} \left\{ 2 J_o(Y) J_1(X) - 2J_2(Y) \left[J_5(X) - J_3(X) \right] \right.$$

$$\left. -j\, 2J_1(Y) \left[J_1(X) - J_3(X) \right] \right\} \tag{30}$$

It is not reasonable to proceed further analytically since the substitution of expression (30) into Equation (21) results in untenable integrals.

Assuming, as previously done, that F(Z) is close to unity magnitude and not changing rapidly, then it is further assumed that

$$F(Z) \approx e^{j\theta(Z)} \tag{31}$$

It follows from Equation (31) that

$$\left| \frac{dF}{dZ} \right| = \left| \frac{d\theta}{dZ} \right|, \tag{32}$$

and if it is assumed that $\frac{d^2F}{dZ^2}$ is zero, then Equations (13) and (32) give

$$\left| \frac{d\theta}{dZ} \right| \approx \frac{K_c}{4c K_o} \left| \frac{I_1}{I_o} \right|. \tag{33}$$

Later solutions will show that θ is monotonic increasing so there is no difficulty in equating the absolute value of the derivative to the derivative of the absolute value of θ or

$$\frac{d|\theta|}{dZ} = \left|\frac{d\theta}{dZ}\right| \tag{34}$$

Using expression (34) in Equation (33) and integrating produces the final approximate equation for θ:

$$|\theta| \approx \frac{K_c}{4c\,K_o} \int_o^Z \left|\frac{I_1}{I_o}\right| dZ \tag{35}$$

Figure 4-1 presents the results of the calculation of $\left|\frac{I_1}{I_o}\right|$ from Equation (30) for three values of c. Each curve is plotted to a value of Z at which the approximation begins to become inaccurate. Because the integral of each curve is used, the inaccuracies at large values of Z do not greatly affect the calculation of $|\theta|$. Notice also that all three curves, in Figure 4-1 are essentially the same except for a scaling of the Z axis.

Figure 4-2 shows the value of the integral of $\left|\frac{I_1}{I_o}\right|$ for three values of c used in Figure 4-1. All curves appear to follow a straight line after an initial buildup length. The slope of this line is approximately 0.64. Thus, after the initial build-up length, $\left|\frac{I_1}{I_o}\right|$ is approximately constant and equal to 0.64.

At this point it is worthwhile to check Figure 4-2 and Equation (35) against an experiment. A UHF helix type traveling wave tube was operated with the following parameters

$$\begin{aligned} c &= 0.10 \\ K_c &= 300\ \Omega \\ K_o &= 23.8\ K\Omega \\ Z &= 18.0 \text{ radians} \\ \theta_{observed} &= 24.5^\circ \end{aligned}$$

Equation (35) predicts 0.327 radians or 18.7°. This results in an error of -24%. The inaccuracy in this case can be directly traced to the assumption

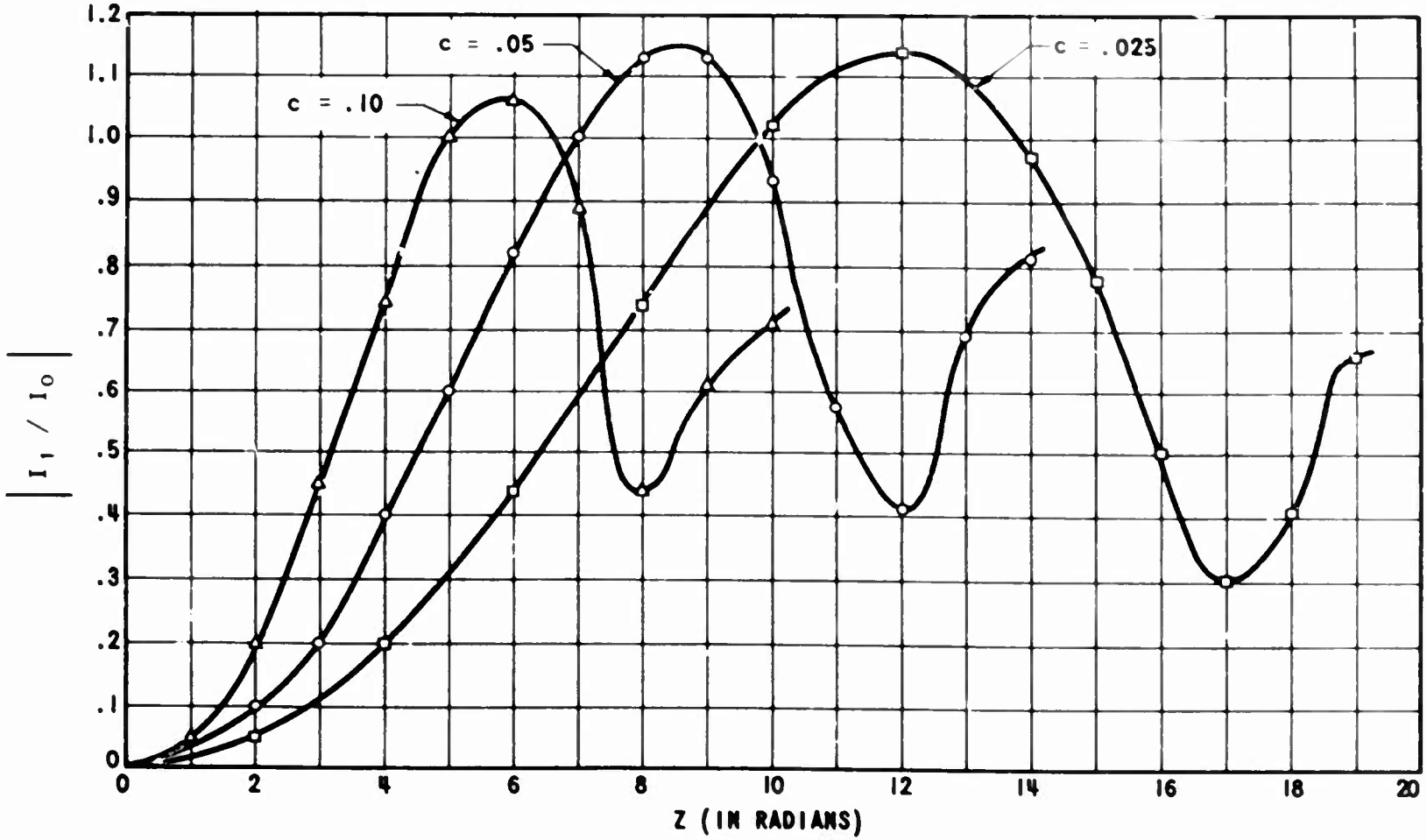

FIGURE 4-1 Calculations of $\left| \frac{I_1}{I_o} \right|$ from Analytical Theory for Three Values of c

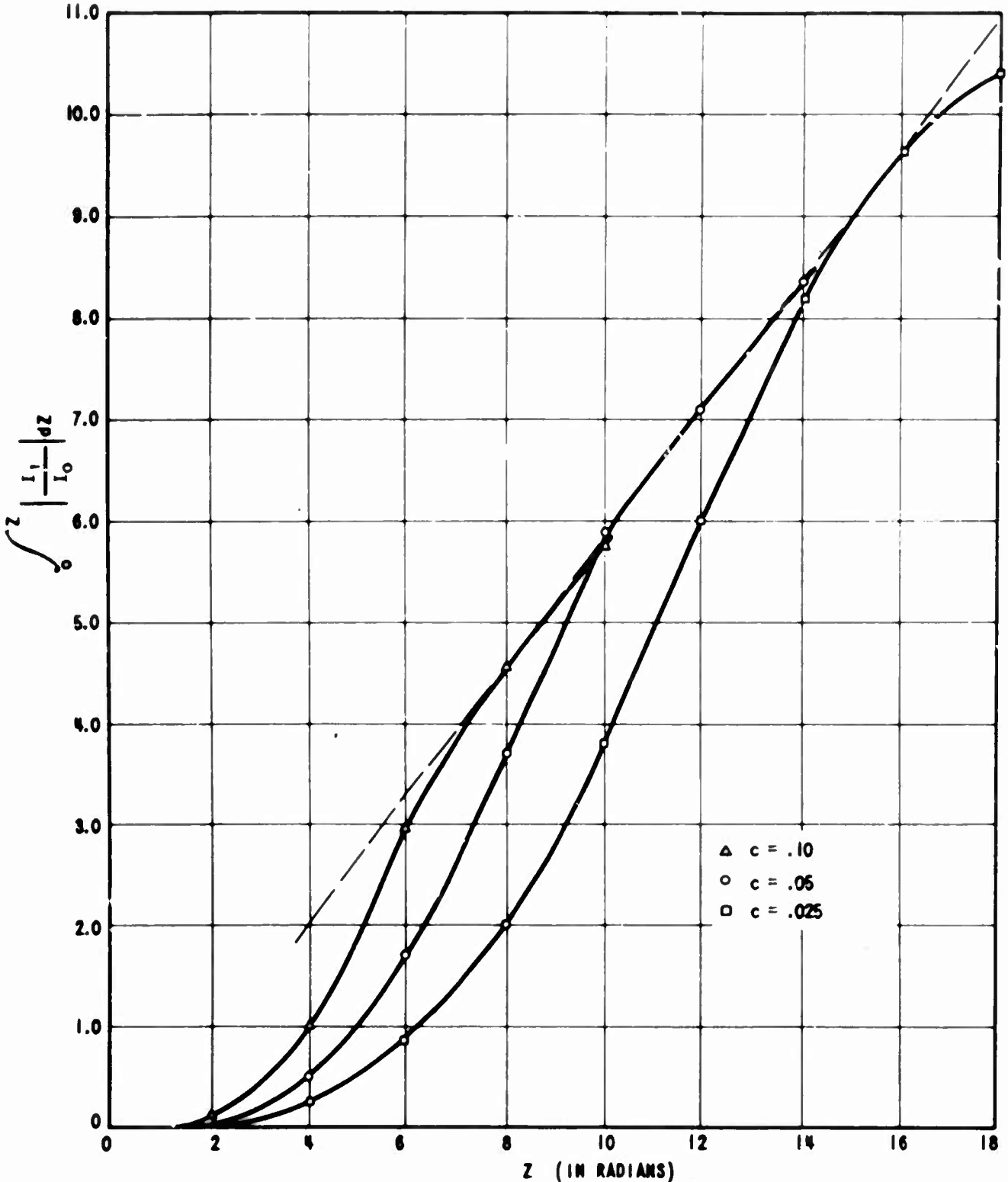

FIGURE 4-2 Value of the Integral $\int_0^Z \left|\frac{I_1}{I_0}\right| dZ$ for Three Values of c

that $\frac{d^2F}{dZ^2} = 0$ in Equation (13). Considering the total circuit length (18.0 radians) the predicted phase shift is quite close to the observed value. That is to say, there are apparently no major errors in the theoretical development or drastic inaccuracies would occur in the calculations. Therefore, Equation (35) with Equation (30) is useful for short devices.

5.0 COMPUTER COMPUTATION OF SOLUTIONS

A program was written and executed on an IBM 7044 Computer for $Z(T, T_s)$, a solution to Equations (3) and (4), for a value of c of 0.10. The computer also performed the inversion process to give $T(Z, T_s)$ for $c = 0.10$ and evaluated the real and imaginary parts of I_1 (See Appendix A). Figure 5-1 presents the results for $\frac{I_1}{I_o}$. Equation (21) for F(Z) can now be evaluated for any given device.

More accurate calculations can now be made for the UHF phase shift device cited earlier. Using the values given in Figure 5-1 in Equation (21) the angle and magnitude of F(Z) were calculated for the same operating conditions mentioned earlier. Figure 5-2 shows these results. The calculation predicts 24.6° phase lag for an 18.0 radian circuit length which is so close to the measured value of 24.5° as to be embarrasing. The closeness is an accident since a correction must still be made for electron space charge. Space charge will only decrease the calculated phase shift by 4%. (See Appendix B)

Figure 5-2 also predicts an amplitude change with circuit length; however, this effect is not large. Both amplitude and phase with vary with beam current. Figure 5-3 shows the calculated variation of phase with beam current obtained simply by allowing K_o to change in Equation (21). Notice that the predicted phase shift is almost exactly linear which agrees with the experimental observations.

The first trial solution for the hot circuit fields is then in reasonable agreement with experimental measurements on the short UHF device. In addition, the substitution of this solution back into Equation (1) would not lead to a very different second solution since the total amplitude and phase changes are quite small.

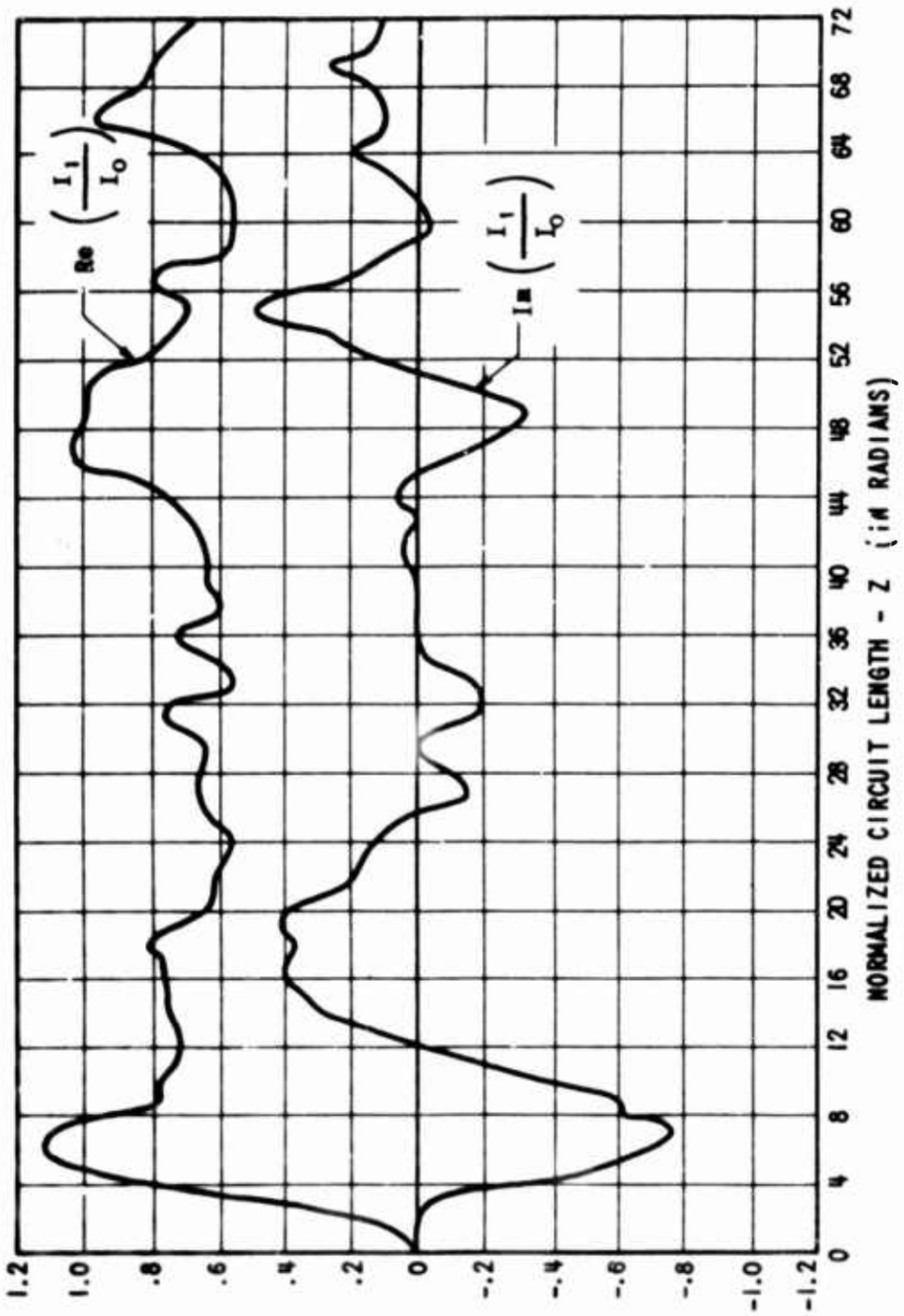

FIGURE 5-1 Computer Computation of I_1 / I_0

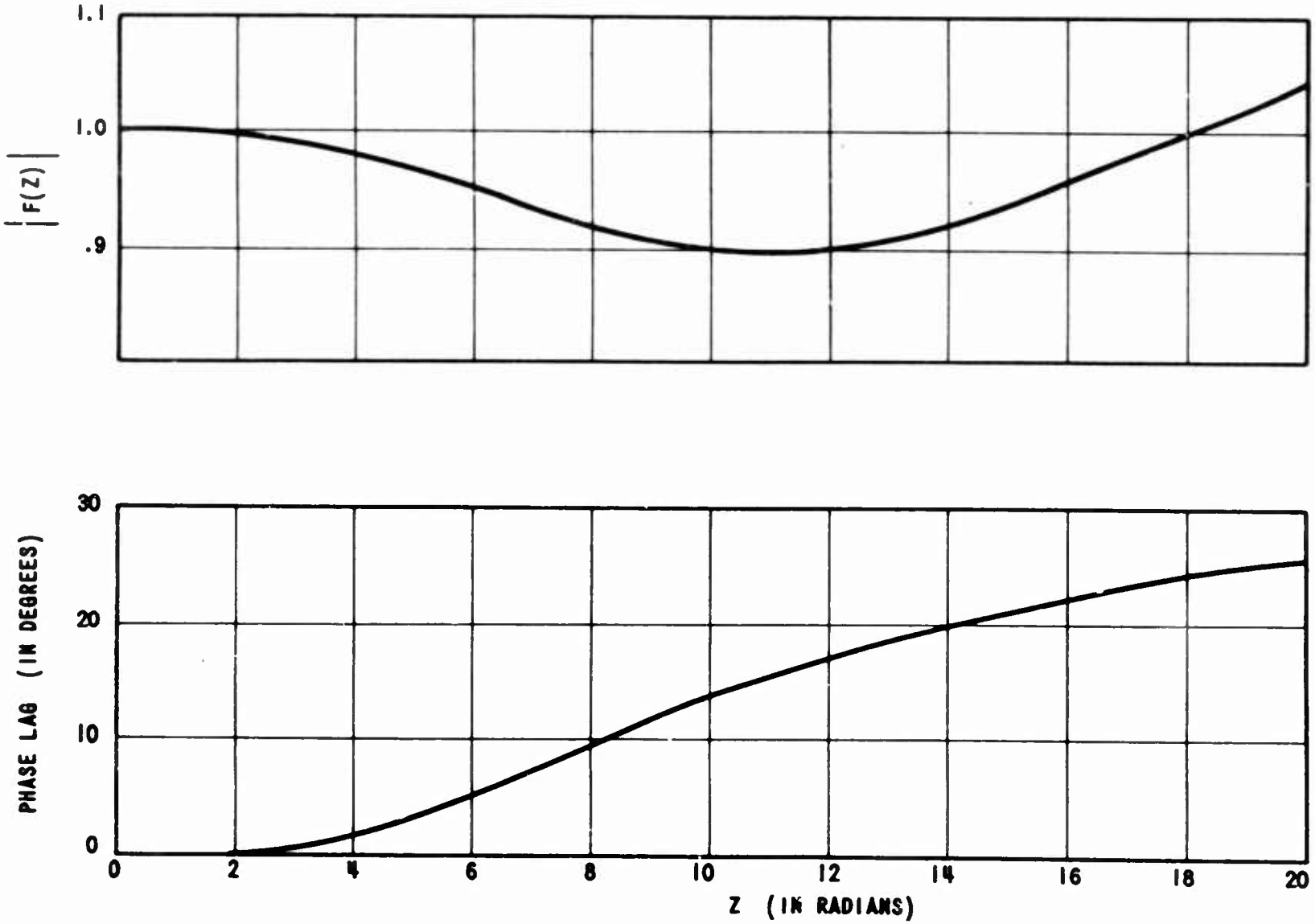

FIGURE 5-2 Ballistic Calculation of Phase Shift Properties for UHF Device

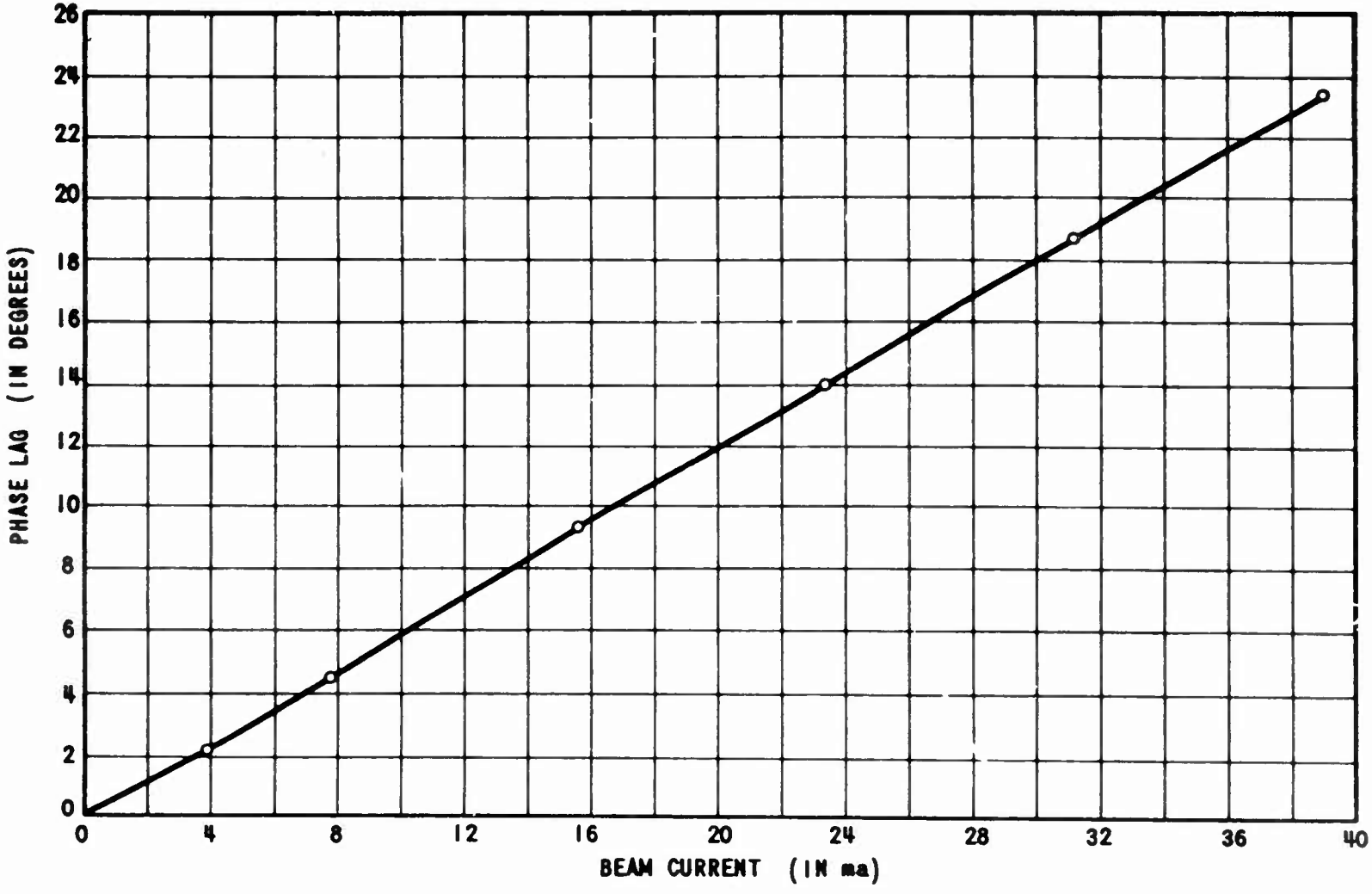

FIGURE 5-3 Calculated Phase Shift as a Function of Beam Current for UHF Device

The situation is considerably different when the first trial solution is found for relatively long slow wave structures. An electron beam phase shifter was constructed for S-band operation, using a circuit of 72.2 radian length. The operating parameters were

$$K_c = 125\ \Omega$$
$$K_o = 9.0\ K\Omega$$
$$c = 0.10$$

The results of calculations, using Figure 5-1 and Equation (21) are shown in Figure 5-4. Two difficulties are apparent from Figure 5-4. The first trouble is seen to be the prediction of gain. For this example the beam power is approximately 60% of the drive power so voltage gain greater than $\sqrt{1.6} = 1.255$ must be non-physical. Likewise the phase calculation predicts that the phase shift increases very slowly after 30 radians and will never reach 90° no matter how long the circuit (assuming that the I_1/I_o solution remain similar for $Z > 70$ radians). It must be concluded that this trial solution is not accurate for long circuits and a second trial solution is needed by using the first trial solution in Equation (1). The next discussion will describe the derivation of a more accurate solution by this procedure.

Where the previous solutions have been accurate they have shown the principle effect of the ac beam current is to produce a phase increase which is nearly proportional to circuit length. This basic property will be used to generate a more accurate solution. The increase in phase shift can be represented as an increase in the circuit propagation constant. Call this increase $\Delta\beta$, then the "hot" circuit field is better approximated by

$$E_z(z,t) = -E_o \sin[\omega t - (\beta_o + \Delta\beta)z] \qquad (36)$$

where $\Delta\beta$ is yet to be determined but assumed constant. By defining

$$\beta_o' = \beta_o + \Delta\beta$$
$$Z' = \beta_o' z \qquad (37)$$
$$T = \omega t,$$

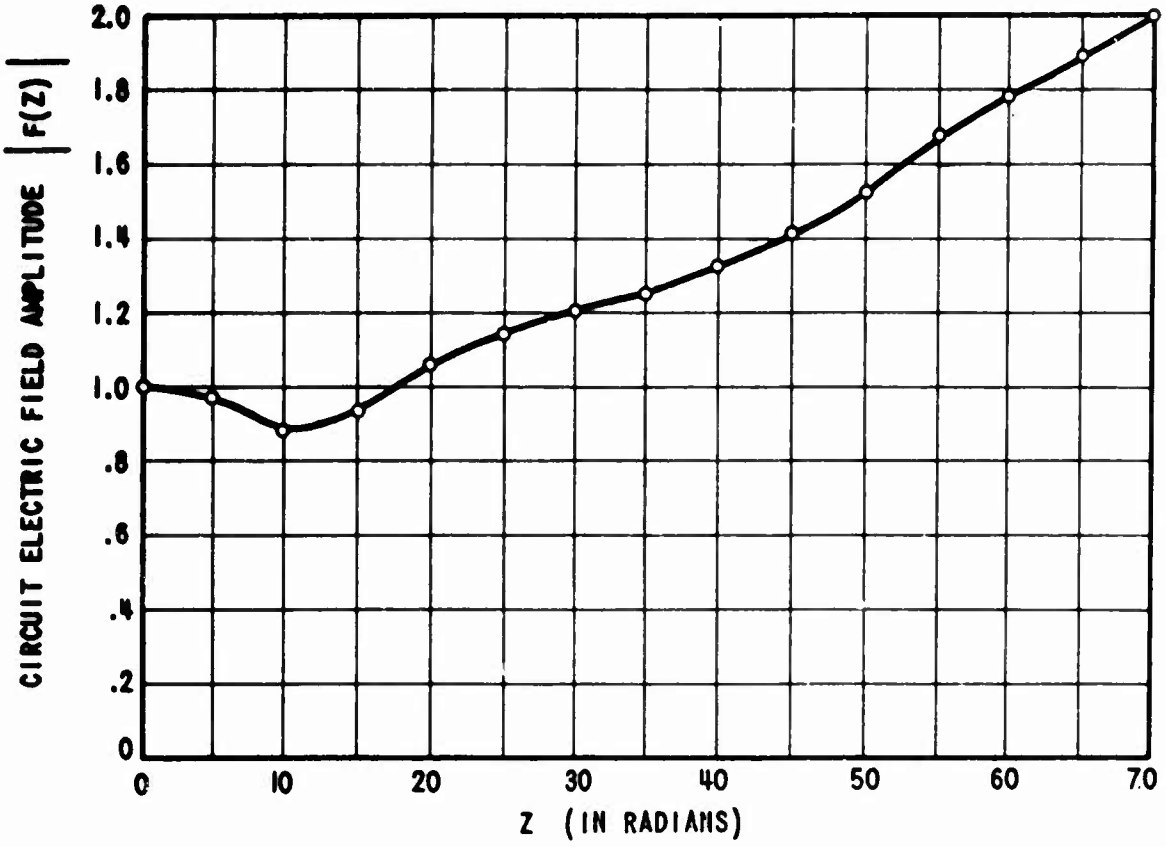

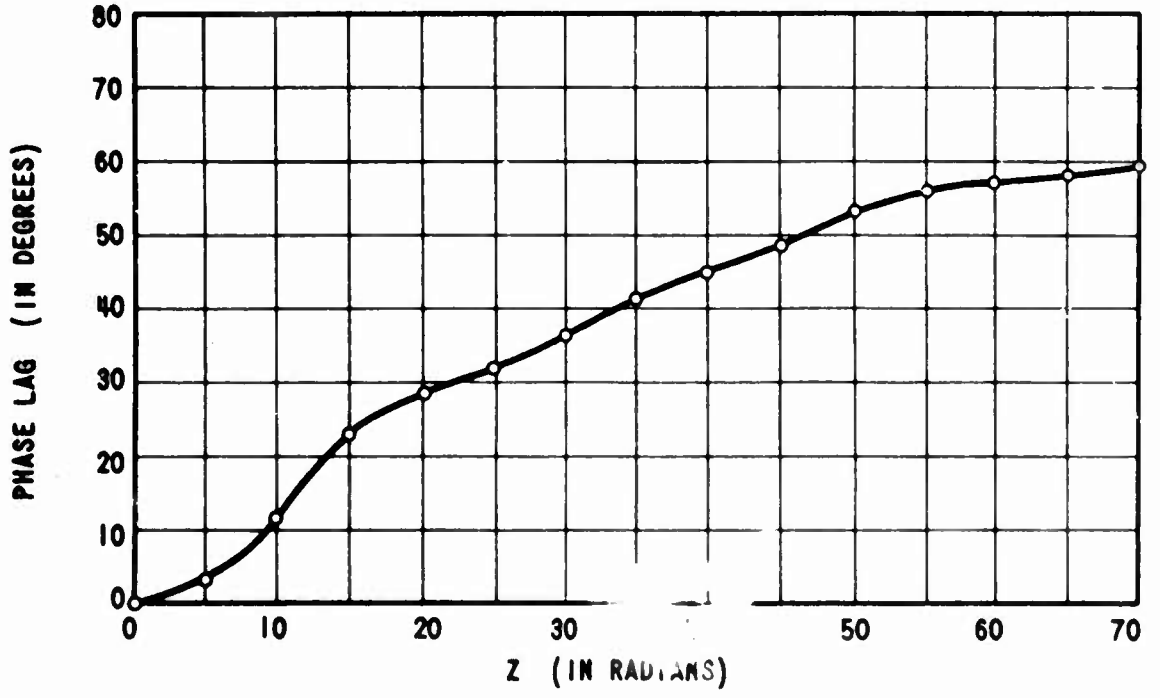

FIGURE 5-4 Calculated Phase Shift Properties of S-Band Phase Shifter

the equation of motion (1) becomes

$$\frac{d^2Z'}{dT^2} = c' \sin (T-Z') \tag{38}$$

where

$$c' = \frac{|e|\ \beta_o'\ E_o}{m_e\omega^2} \tag{39}$$

At time $T = T_s$, the starting time, $Z = 0$ and

$$\frac{dZ'}{dT} = \frac{\beta_o'}{\omega}\ u_o \tag{40}$$

If u_o is not set equal to the cold circuit phase velocity ($\frac{\omega}{\beta_o}$) but instead lowered to a velocity $\frac{\omega}{\beta_o'}$ (which is approximately the "hot" phase velocity) then

$$\left.\frac{dZ'}{dT}\right|_{\substack{Z'=0 \\ T=T_s}} = 1, \tag{41}$$

and phase shift should be maximized. In addition, the last assumption on velocity allows use of the previous computer solution (Figure 5-1) since Equations (38) and (41) are exactly the same as Equations (3) and (4).

An approximate value of $\Delta\beta$ must first be determined. The circuit electric field and ac beam current are given as

$$\begin{aligned} E_z(z,t) &= j\frac{E_o}{2}\, e^{j(\omega t-\beta_o' z)} - j\frac{E_o}{2}\, e^{-j(\omega t-\beta_o' z)} \\ i_z(z,t) &= -\frac{I_1}{2}\, e^{j(\omega t-\beta_o' z)} - \frac{I_1^*}{2}\, e^{-j(\omega t-\beta_o' z)} \end{aligned} \tag{42}$$

Putting these expressions into Equation (8) and equating imaginary parts give

$$(\beta_o')^2 - \beta_o^2 = \frac{\beta_o(\beta_o')^2 K_c}{E_o} \, Re(I_1). \tag{43}$$

Using expression (39) and the fact that $\frac{m}{e} u_o^2 = 2 V_o$, $u_o = \frac{\omega}{\beta_o'}$, and $K_o = \frac{V_o}{I_c}$, Equation (43) becomes

$$(\beta_o')^2 - \beta_o^2 = \frac{\beta_o \beta_o' K_c}{2c' K_o} \, Re(\frac{I_1}{I_o}). \tag{44}$$

Define the constant ϕ as

$$\phi = \frac{\Delta\beta}{\beta_o} \tag{45}$$

If β_o' in Equation (44) is expressed in terms of ϕ and β_o and the equation solved for ϕ, the result is

$$\phi = \frac{K_c}{4c' K_o} \, Re(\frac{I_1}{I_o}) \tag{46}$$

This result says essentially the same thing as Equation (35). Figure 5-1 shows that the value of $Re(\frac{I_1}{I_o})$ is essentially constant as a function of Z' for Z' larger than 8 radians. Thus ϕ can be taken constant and good accuracy maintained.

With ϕ evaluated, it is possible to find the second trial solution for E_z. The electric field is assumed as before to be

$$E_z = j \frac{E_o}{2} F(Z) e^{j(T-Z)} - j \frac{E_o}{2} F^*(Z) e^{-j(T-Z)}, \tag{47}$$

where the prime is not used on Z since F(Z) is defined to include the first order phase shift. The fundamental component of ac beam current is given by Equation (42) and can be written as

$$i = -\frac{I_1}{2} e^{-j\phi Z} e^{j(T-Z)} - \frac{I_1^*}{2} e^{j\phi Z} e^{-j(T-Z)} \qquad (48)$$

Substiution of Expressions (47) and (48) into the circuit Equation (9) produces

$$j\frac{d^2F}{dZ^2} + 2\frac{dF}{dZ} = -j\frac{(1+\phi)K_c}{2c'K_o}\frac{I_1}{I_o} e^{-j\phi Z} \qquad (49)$$

Following the same procedure as used for Equation (13), the expression for F(Z) can be shown to be approximately

$$F(Z) = 1 - j\frac{(1+\phi)K_c}{4c'K_o}\int_o^Z \frac{I_1}{I_o} e^{-j\phi Z} dZ - \frac{(1+\phi)K_c}{8c'K_o}\frac{I_1}{I_o} e^{-j\phi Z} \qquad (50)$$

Equation (50) now enables calculation of a second trial solution for F(Z) for the particular condition of beam velocity below cold circuit synchronism. The accuracy will be considerably better than previously obtained. It is a simple task to show that Equation (50) predicts low insertion loss (or gain) for circuits of length greater than 8 radians. Consider the example where I_1/I_o is approximately a real constant and using Equation (46), Equation (50) can be shown to be

$$F(Z) \approx 1 - j(1+\phi)\phi \int_o^Z e^{-j\phi Z} dZ - (1+\phi)\frac{\phi}{2} e^{-j\phi Z}, \qquad (51)$$

which is easily shown to be

$$F(Z) \approx (1 + \frac{\phi}{2}) e^{-j\phi Z} - \phi. \qquad (52)$$

Because ϕ is typically smaller than 0.10, the phase of F(Z) is approximately $-\phi$ and the magnitude of $|F(Z)|$ is close to unity. The new solution satisfies the original assumptions regarding the electric field and must therefore be quite accurate. The new solution describes operation near "hot" circuit synchronism and should then give the maximum phase shift.

As an example, the S-band device mentioned earlier was considered. The value of Re (I_1/I_o) was taken as 0.65 and ϕ found to be 0.0226. $I_1/I_o e^{-j\phi Z}$ was computed from Figure 5-1 and is shown on Figure 5-5. Computation using Equation (50) produces the results shown in Figure 5-6. The magnitude of the circuit electric field remains within 20% of unity and its phase is nearly a linear function of circuit length. The phase shift predicted for a circuit length of 72 radians is 96° whereas about 80° was measured. Some part of this error will be eliminated when the correction due to space charge is made. It is seen in Appendix B that the correction amounts to a reduction in phase shift by 7%. The calculated phase shift is then 89.6°. The actual insertion gain would probably be reduced by circuit losses (not included in the calculation) and was not measured. Figure 5-7 shows that as beam current is varied the calculated phase shift is still nearly a linear function although definite deviation from linearity is present.

It is useful to evaluate further the simple approximation for phase shift, ϕ. From Figure 5-1, a value of Re (I_1/I_o) can be taken as 0.65. The phase shift indicated by Equation (46) is then

$$\phi Z = \frac{0.65\, K_c Z}{4c' K_o} \tag{53}$$

This result is the same as Equation (35) applied to long structures. Note that the value of $\left|I_1/I_o\right|$ determined from Figure 3 was 0.64.

Using the definition of c', K_o, u_o, and Pierce impedance, Equation (53) is easily shown to express the phase lag near synchronism per unit length of slow wave structure as

$$\frac{0.325\pi}{\sqrt{\frac{|e|}{m_e}}}\; f\; I_o \sqrt{\frac{K_c}{V_o P_{rf}}} \tag{54}$$

Notice that expression (54) says that phase shift is proportional to the average beam current and inversely proportional to rf drive power. Both effects are observed in experiments (See Appendix C for comparison of Equation (54) with the earlier design equation).

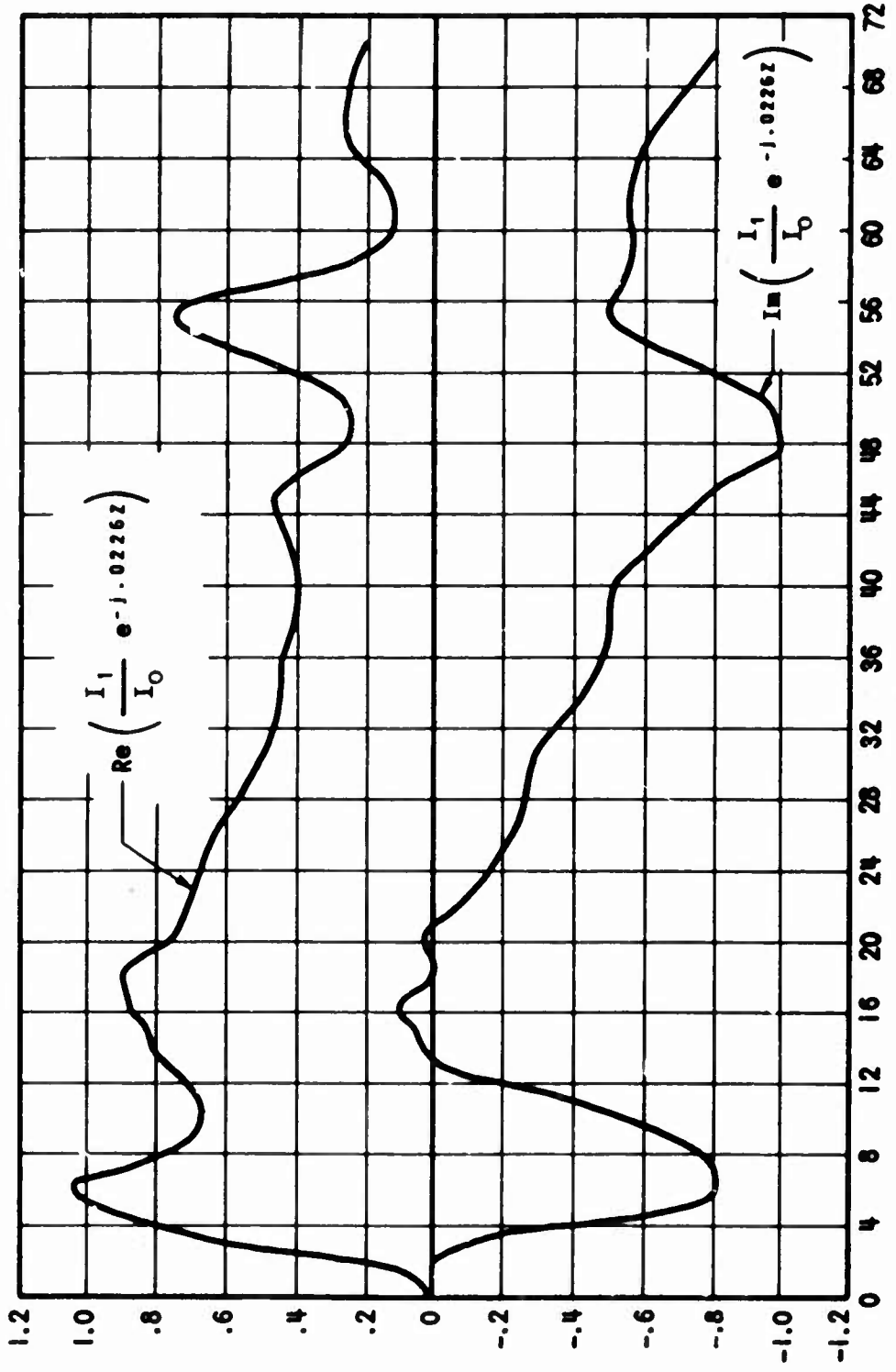

FIGURE 5-5 Calculated Values of $\frac{I_1}{I_0}\, e^{-j.02262}$

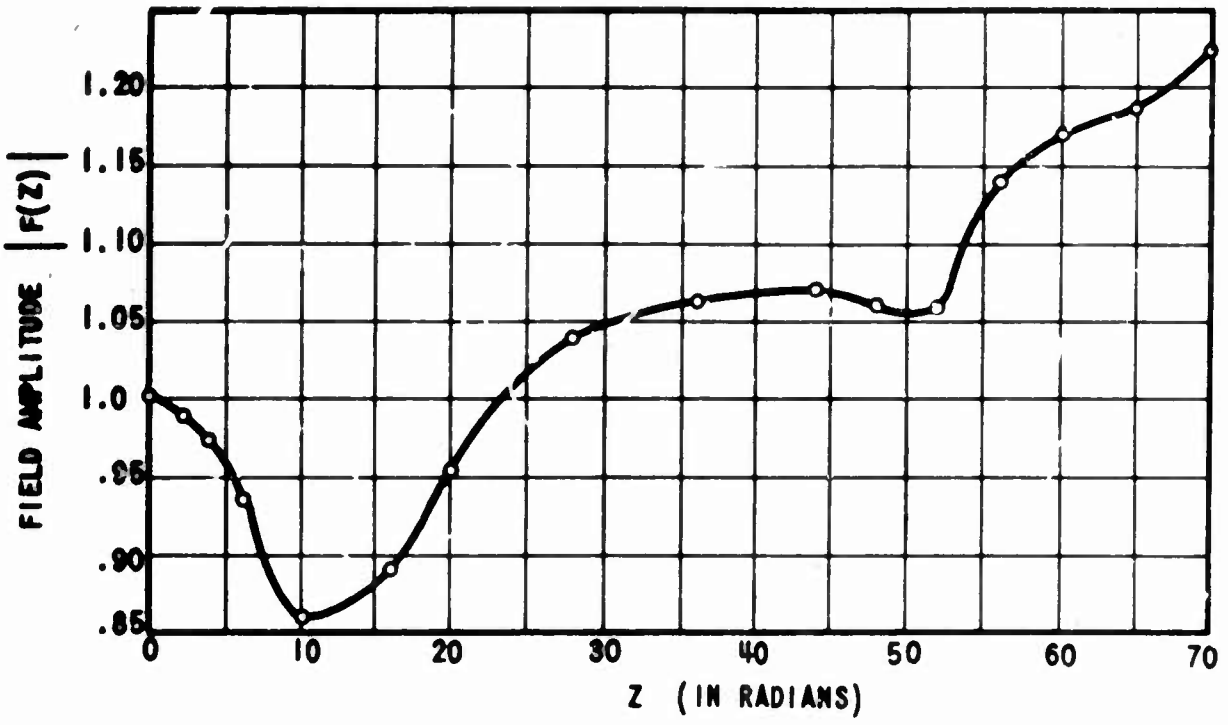

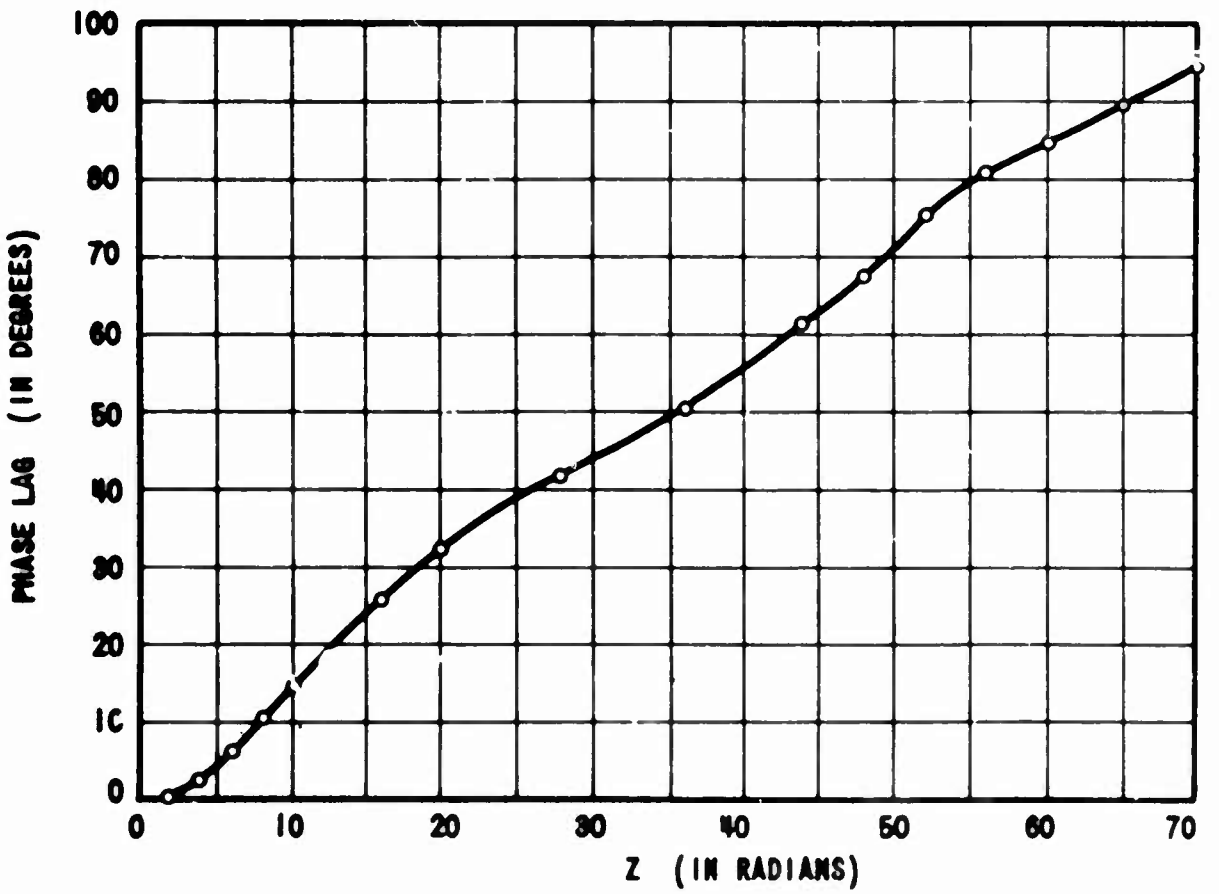

FIGURE 5-6 Calculated Characteristics of S-Band Phase Shifter for $u_o / v_c = .974$, $c = .10$

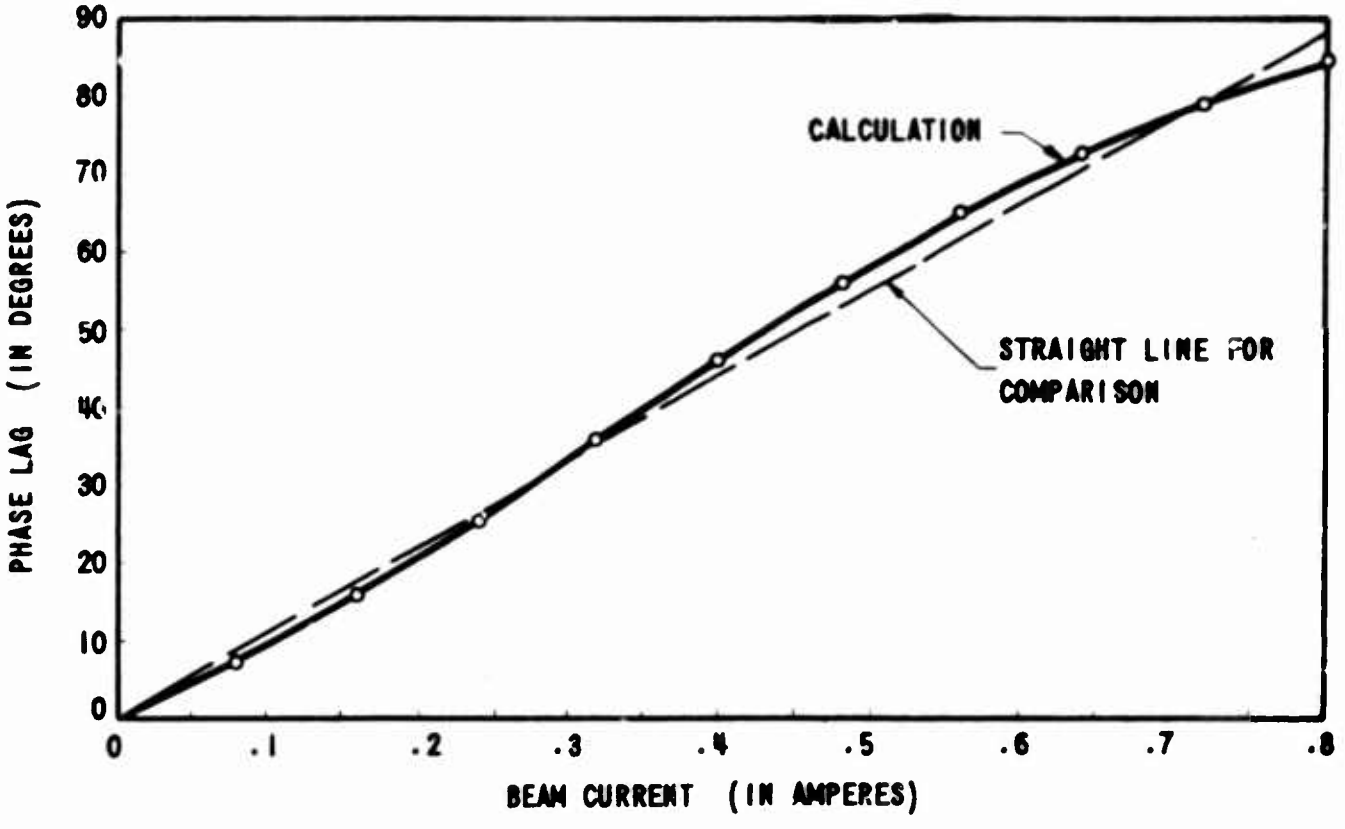

FIGURE 5-7 Calculated Phase Lag vs Beam Current for S-Band Device at u_o/v_c = .974, c = .10, Z = 60 Radians

6.0 COMPARISON OF CALCULATIONS AND EXPERIMENTS

Although considerable data is available for each of the three phase shifter devices constructed, a comparison between experiments and theory will be made for typical operating conditions. In each case the dc beam voltage is adjusted for maximum phase shift. This comparison is made in Table 1. The design equation used for each of these tubes is essentially Equation (44) and it had been developed independently from a perturbation theory assuming that the ac current solutions are regular. The computer computation gives the ac current solutions to good accuracy and verifies this assumption. Equation (53) is therefore believed to be sufficiently accurate for long circuits to alleviate the need for an extensive computer study. The computer computations made enabled verification of the simple design criteria which simply state that large phase control results from using long circuits, high beam perveance, and large Pierce impedance circuits. To achieve 360° at S-band proves to be the practical problem of finding the best electron gun and circuit, rather than a theoretical problem.

TABLE 1

Device	f_o Mc	V_o V	I_o A	K_c Ω	Z RAD.	P_{RF} W	$\frac{K_c}{4cK_o}$	Phase Shift in Degrees		
								Obs.	Eq.* (53)	Eq.* (50)
UHF	600	930	0.039	300	18.0	65	0.0314	24.5	19.9	23.5
						250	0.0160	12.0	10.2	12.0
S	2,800	7,200	0.80	125	72.2	10,000	0.0347	80.0	86.9	89.6
L	1,350	10,500	6.0	100	73.7	65,000	0.0803	215.0**	208.0	229.0

* Including reduction due to space charge given by Appendix D.

** The agreement between theory and experiment is probably not as good as indicated because the value of Pierce impedance is uncertain within a factor of two. It was possible in these experiments to achieve 290° at 5.0 amperes by proper adjustment of the magnetic field which controlled the beam focusing and greatly affected the interaction impedance.

7.0 THE EFFECT OF NON-SYNCHRONOUS OPERATION

It was observed in all of the experiments that maximum phase shift occurs at a beam voltage very close to the synchronous voltage (likewise it was demonstrated that no phase control results from feeding rf power in the direction opposite to the electron flow). These observations support the preceding analysis since the basic beam bunching equation assumes synchronism of electron velocity and circuit wave velocity. For quite non-synchronous operation the basic bunching equation would show negligible beam bunching and result in negligible phase shift. No computer calculations were made for general non-synchronous conditions. However, it's simple to derive the analytical solution for short devices, and it does provide insight to the problem.

As discussed previously, the analytical solutions for electron trajectories are only accurate for short slow-wave structures or for the first part of a long structure. However, it can be shown that the synchronism effects at the beginning of a structure are the same type as occur all the way along the structure. Thus, if the phase shift does not initially build up as fast for a non-synchronous condition, the solutions for longer sections continue to show a smaller phase shift per radian of slow wave structure, i.e. no sudden rise in phase shift per radian will occur.

The derivation of non-synchronous operation proceeds in the following manner. Both the circuit electric field and the bunched current are still assumed to be described by $\exp\{j\omega t - j\beta_o z\}$ or $\exp\{jT - jZ\}$; however, the beam velocity, u_o, is not necessarily the same as the cold circuit velocity, v_c (or ω/β_o). Call

$$k \equiv \frac{u_o}{v_c} \tag{55}$$

and assumes that 1-k is small.

The first approximation for electron motion is then

$$T \approx T_s + \frac{Z}{k} \tag{56}$$

and the entrance condition is:

$$\left.\frac{dZ}{dT}\right|_{\substack{Z=0 \\ T=T_s}} = k \tag{57}$$

The equation of electron motion is again Equation (3):

$$\frac{d^2Z}{dT^2} = c \sin (T-Z) \tag{3}$$

The right hand side can be expanded in powers of $(T-T_s)$ and the 2nd order solution for Z is found to be

$$Z \approx k(T-T_s) + \frac{c \sin T_s}{2}(T-T_s)^2 + \frac{(1-k)c}{6}(T-T_s)^3 \tag{58}$$

where terms involving $(1-k)^2$ have been dropped since $(1-k)$ is small. The inversion of the last equation gives

$$T-T_s \approx \frac{Z}{k} - \frac{c \sin T_s}{2k^3} Z^2 + \left[\frac{c^2 \sin^2 T_s}{2k^5} - \frac{(1-k)c}{6k^4} \cos T_s\right] Z^3 \tag{59}$$

The expression T-Z can now be approximated and the value of the beam current at the fundamental frequency is found to be approximately

$$\frac{I_1}{I_o} \approx e^{-jY'} \left\{2J_1(X) + jY[J_3(X) - J_1(X)]\right\} \tag{60}$$

or

$$\mathrm{Re}\left(\frac{I_1}{I_o}\right) \approx 2J_1(X) \cos Y' + [J_3(X) - J_1(X)]\, Y \sin Y' \tag{61}$$

$$\mathrm{Im}\left(\frac{I_1}{I_o}\right) \approx -2J_1(X) \sin Y' + [J_3(X) - J_1(X)]\, Y \cos Y'$$

where

$$X = \frac{CZ^2}{2k^3}$$

$$Y = \frac{C^2Z^3}{4k^5} \qquad (61)$$

$$Y' = Y + \frac{2}{3}\left(\frac{1-k}{k}\right) \cdot Z$$

Further analytical derivation will get far too complicated to justify the results. Therefore, to illustrate the effect of k upon the ac beam current and the final phase shift, a set of curves for various values of k have been calculated. Because the expansions are accurate to larger Z if c is smaller, a value of 0.05 is chosen. Figures 7-1 and 7-2 show the results of these current calculations. By comparing these curves with the computer solution for $k = 1.0$, it was estimated that these curves should be accurate for computation of phase for

$$0 \leq Z \leq 7,$$

and the least accuracy occurs in the $k = 0.85$.

A value of $Z = 7.0$ radians will be taken for computation of phase shift. Phase shift is found by calculating the angle of the vector $F(Z)$ where

$$F(Z) = 1 - j\,\frac{K_c}{4c\,K_o}\int_o^Z \frac{I_1}{I_o}\,dZ - \frac{K_c}{8c\,K_o}\,\frac{I_1}{I_o}. \qquad (21)$$

The results of this calculation is given in Figures 7-3 and 7-4 for three values of $K_c/4c\,K_o$.

Figure 7-3 shows that near synchronism the phase shift is larger than well away from synchronism. In addition, as the parameter $K_c/4c\,K_o$ is increased, larger phase shift is observed at a beam velocity slightly below cold

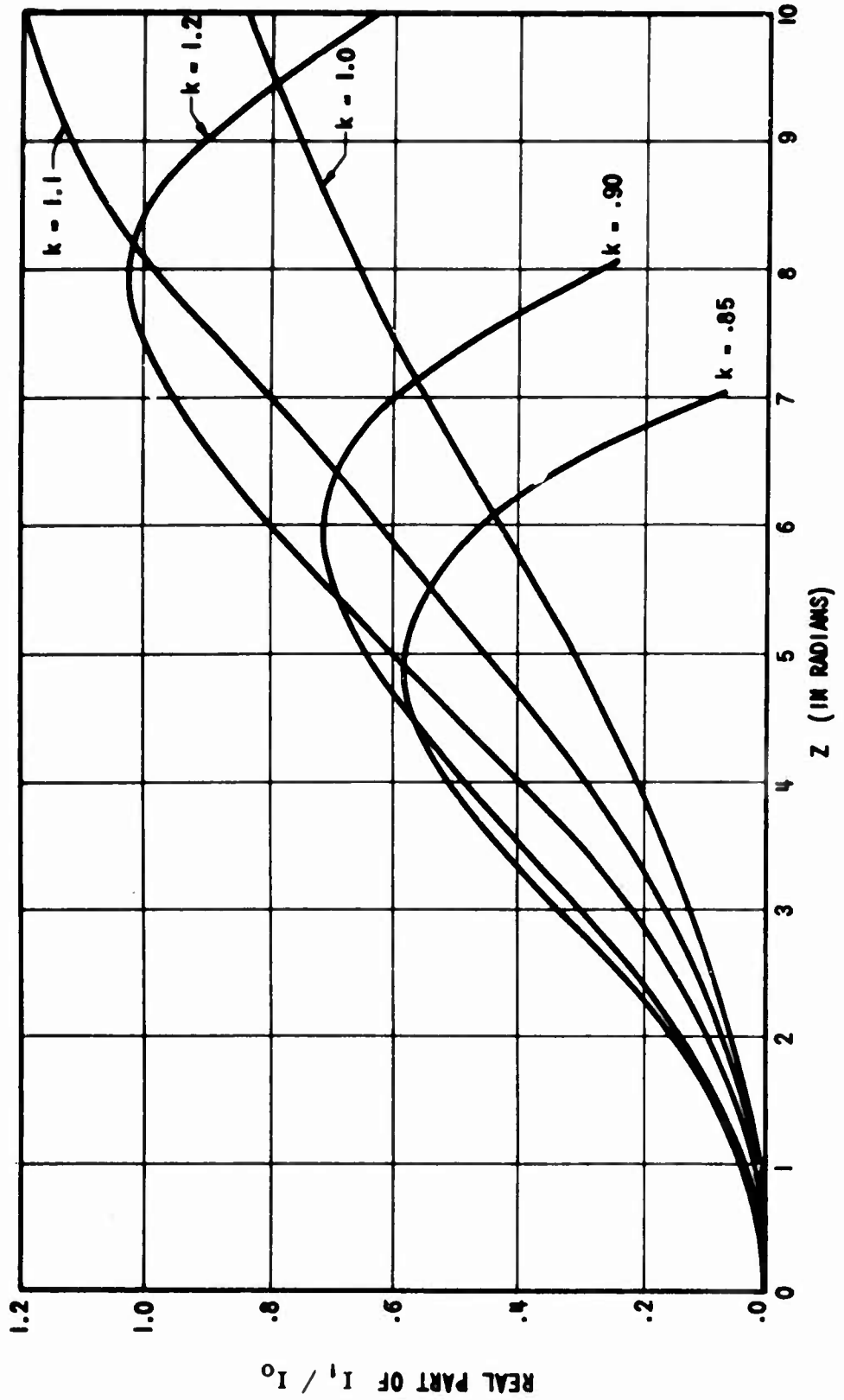

FIGURE 7-1 Calculated AC Beam Current (Real Part) vs Circuit Length for c = .05

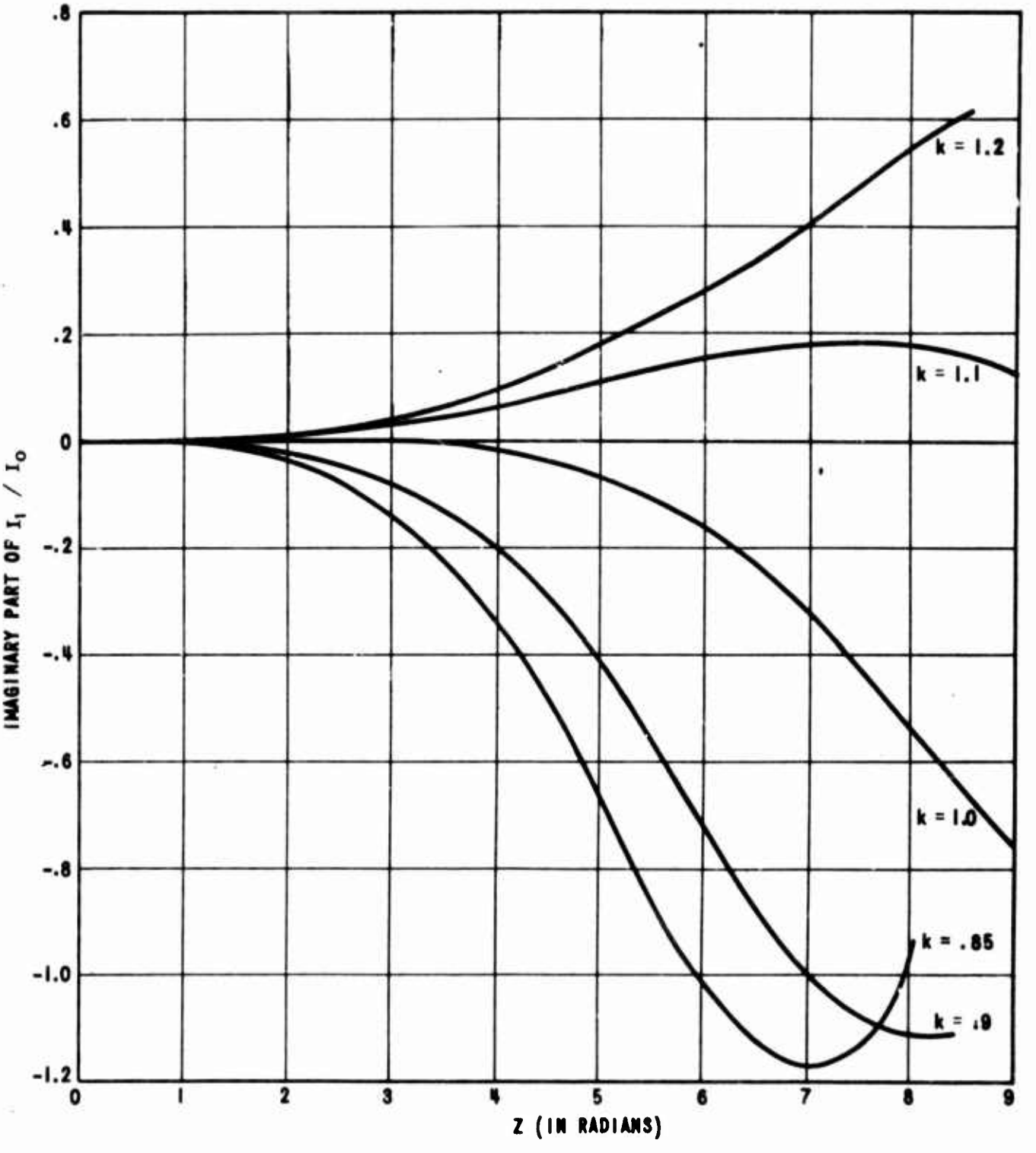

FIGURE 7-2 Calculated AC Beam Current (Imaginary Part) vs Circuit Length for c = .05

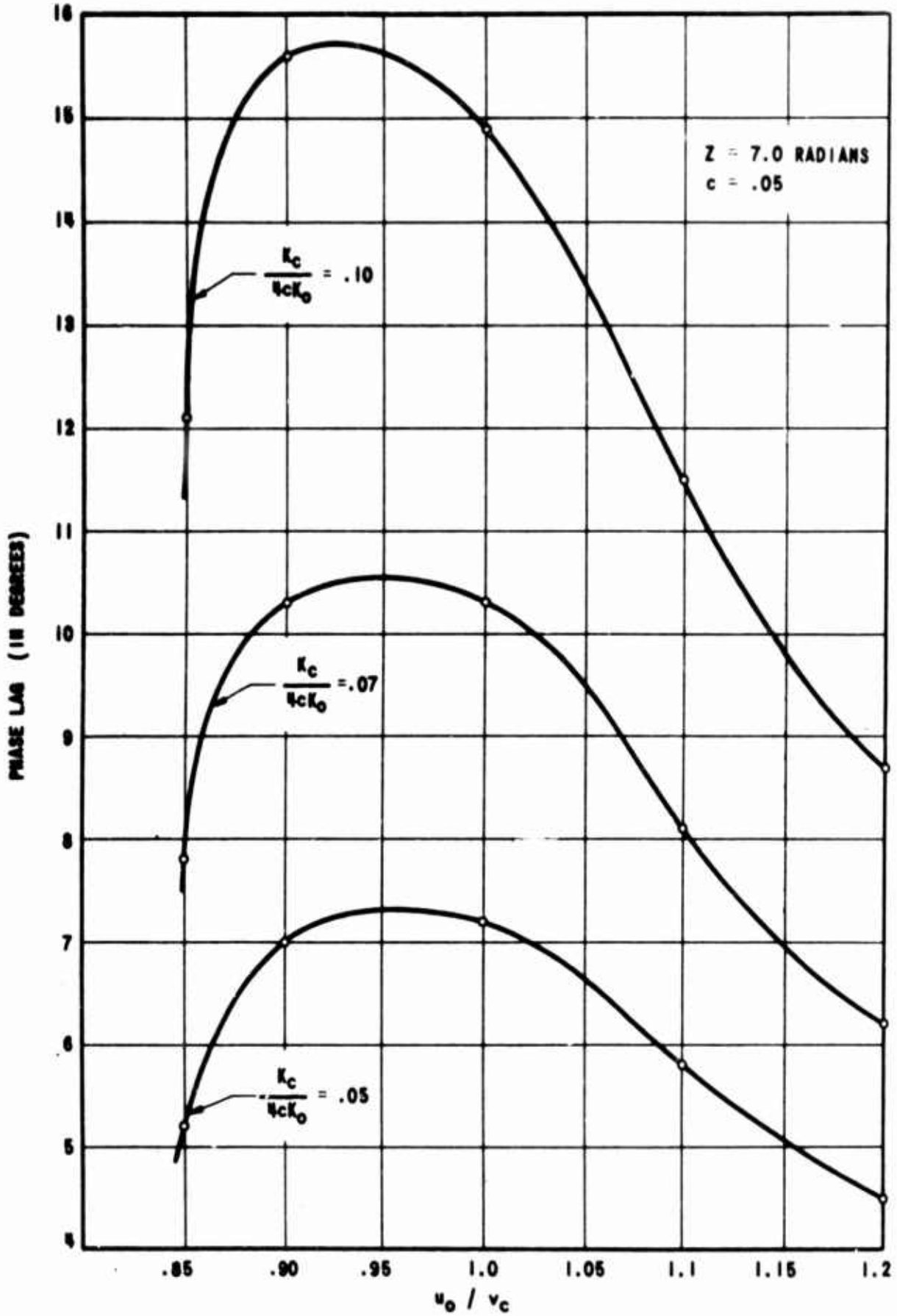

FIGURE 7-3 Calculated Phase Shift vs The Ratio of Beam Velocity to Circuit Wave Velocity

synchronous velocity. Figure 7-4 demonstrates a tendency for insertion gain above synchronism and insertion loss below synchronism and the effect is stronger the larger the value of $K_c/4c\,K_o$. This insertion loss change with beam velocity has been observed but no quantitative data is available. Some data for phase shift as a function of beam voltage is shown in Figure 7-5.

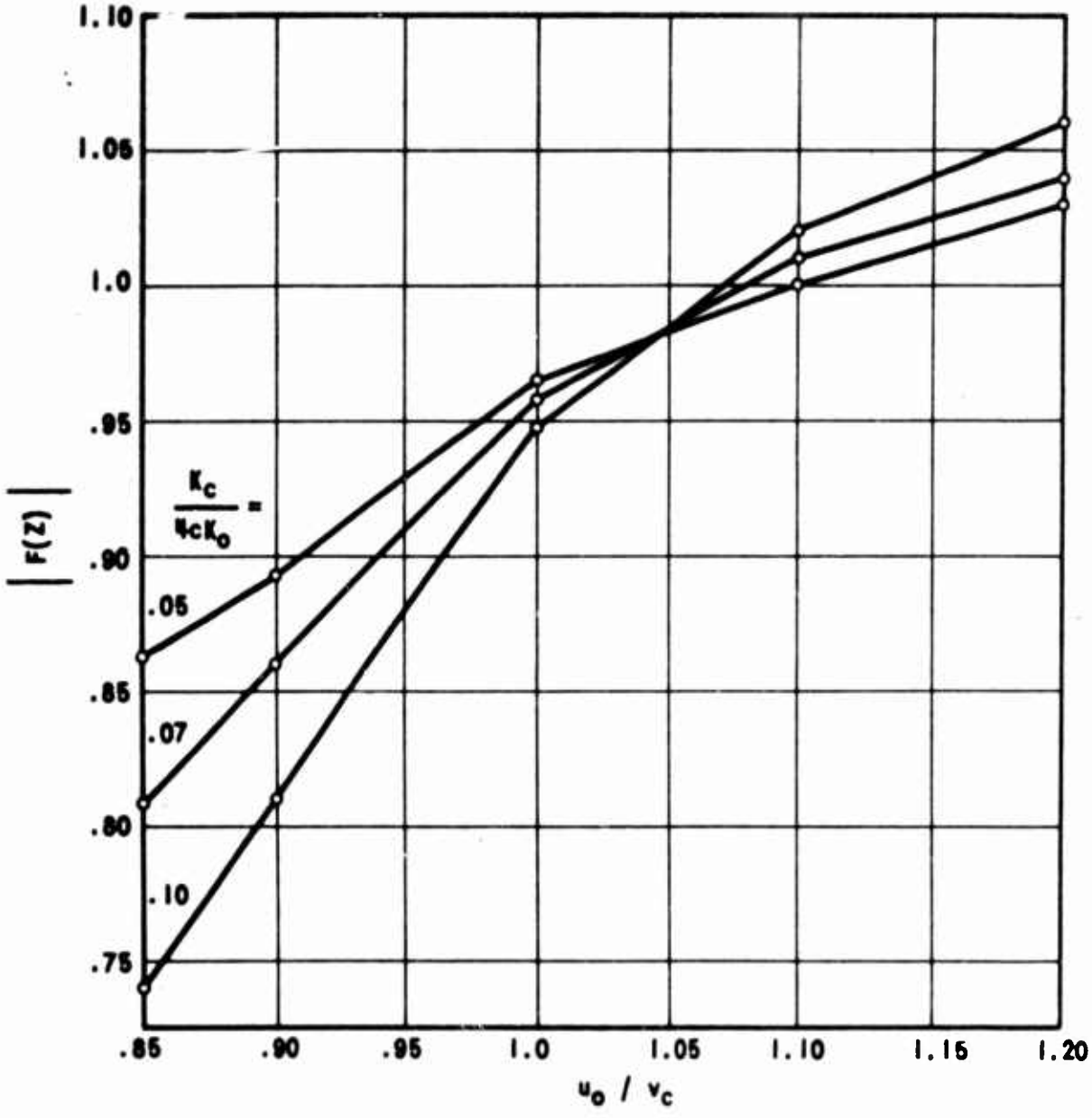

FIGURE 7-4 Calculated Circuit Amplitude vs the Ratio of Beam Velocity to Circuit Wave Velocity for Z = 7.0, c = .05

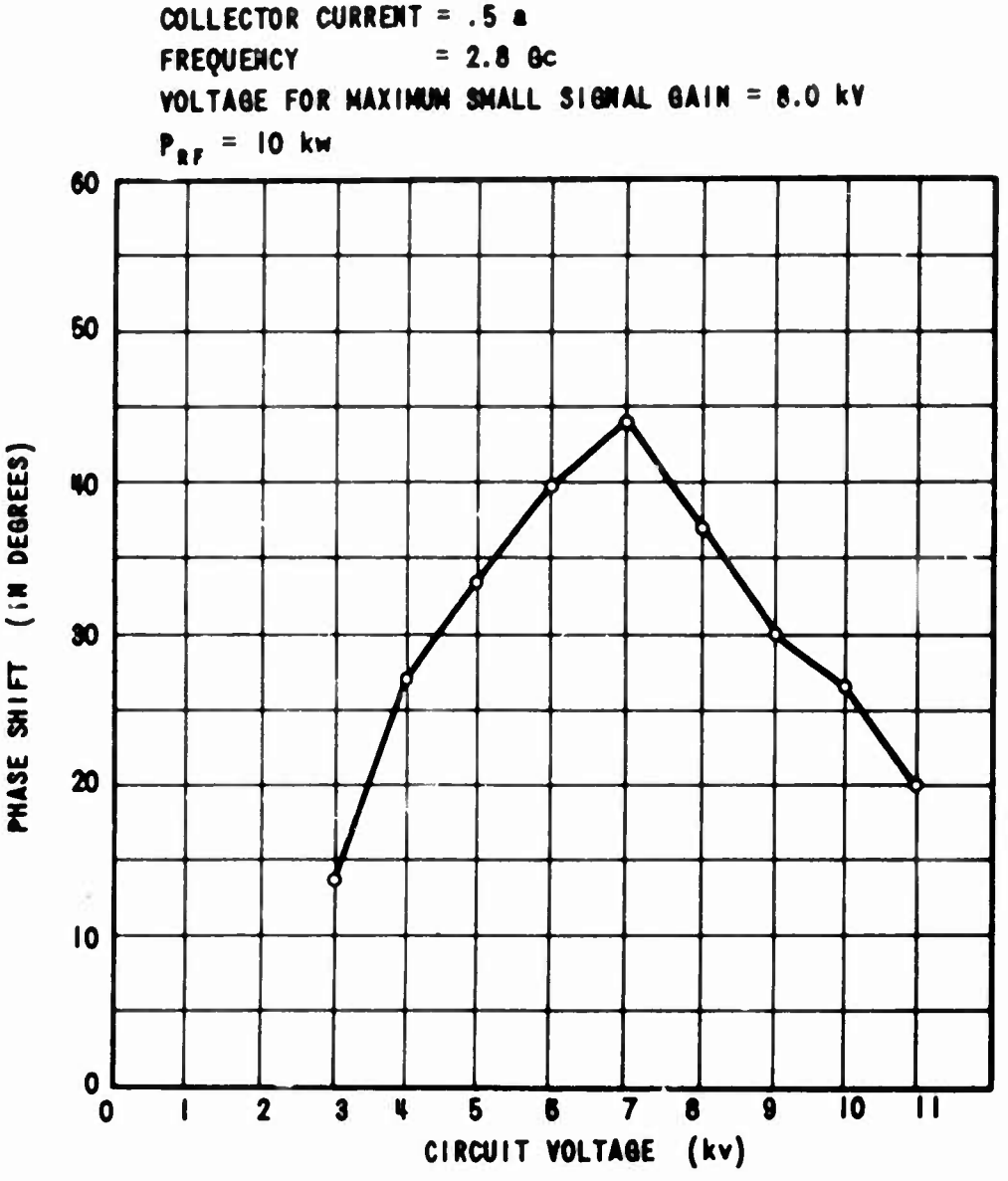

FIGURE 7-5 Phase Shift vs Circuit Voltage for S-Band Device

8.0 OTHER PHENOMENA

All the experimental phenomena mentioned in the introduction have been explained by the preceding analysis except number 7 which relates to two slow-wave sections in a single device. A complete explanation of the effect would involve computer calculation which includes the effect of a short drift region. This has not been done; however, it is expected that such calculation would bear out the following hypothesis. Appreciable ac current is assumed to enter the second structure. Because the external phase length between the output of the first structure and the input of the second structure is variable, the rf drive power for the second structure can be adjusted for any arbitrary phase with respect to the entering ac beam current. Equation (9) shows that the ac current will induce a circuit voltage of a certain phase which is again of arbitrary phase with respect to the rf drive signal. By considering the energy exchange process it seems clear that the ac beam current will automatically adjust its phase for reactive loading or the production of phase shift similar to the first section.

The reasoning is as follows. Electron entering in a phase to induce energy into the circuit will do so and slow down. Likewise electrons entering in a phase to extract energy from the circuit will do so and speed up. Because the circuit fields and energy are quite large compared to the beam energy it is probable that only a short length is needed for the effect to be completed and for the electron to be "captured" by the rf circuit fields. Once captured, the same type of electron ballistics will occur in the second section as occurred in the first section and phase control will be observed.

Because the electron beam in the phase shifter is operated in an "over-saturated" condition, many non-linear phenomena will be present that could be

more important than usual in TWT's. The most obvious effect is the generation of harmonic power within the beam which can be coupled to the device's output if the slow-wave circuit has appreciable Pierce impedance at harmonic frequencies. Equation (6) allows calculation of the harmonic current, and the values will probably be large since bunching is strong the whole length of the device. No experimental data is available; however, one expects that long devices will have worse harmonic output than short devices. A "worst case" estimate was made for the S-band helix type phase shifter, and the result was second harmonic power 6 db below the fundamental and third harmonic power 15 db below the fundamental (see Appendix D).

The other difficulty of non-linear operation is that strong mixing effects will occur. Multi-frequency operation will produce disastrous amounts of cross-modulation and intermodulation. Unless the modulation rates are low, strong AM to PM conversion will also occur. For some phase array radar systems this may present no problems.

9.0 CONCLUSION

It was shown that the ballistic equations of motion coupled with the circuit equation for induced voltage produced accurate solutions for phase shift in the electron phase shifter. A computer solution was shown to be accurate for long circuits and several analytical solutions were derived for short circuit lengths. A simple design equation was verified as being reasonably accurate for most cases.

The phase shifter is not a "fast wave" device in the sense that the TWT is a "slow wave" device. Qualitatively, it is a device that produces phase shift by the reaction of bunched electron current upon the circuit field. The fundamental component of electron current induces a voltage approximately 90° phase lagging the original circuit voltage that caused electron bunching. Operation near synchronism allows a strong fundamental component throughout the device and in such a phase as to produce an increasing phase lag of the circuit fields. Operation well removed from synchronism produces negligible phase shift. Because all the phenomena observed in these devices can be explained with this simple model, it is felt that no fundamental principle of operation has been overlooked. Thus difference between devices employing different slow-wave structures and electron guns will depend mainly upon the beam perveance, Pierce impedance, and the drive power level much like the design of TWT's.

APPENDIX A

COMPUTER SOLUTION BY J. MYERS

The actual program executed by J. Myers found the ac current defined by

$$I_{ac} = \int_{0}^{2\pi} e^{-jT} \, dT_s \qquad \text{(A-1)}$$

which is different than I_1 defined in the text. The computer solution for I_{ac} is shown in Figure A-1. Figure 5-1 of the text was computed from Figure A-1 by use of the relation:

$$\frac{I_1}{I_o} = \frac{I_{ac}}{\pi} e^{jZ} \qquad \text{(A-2)}$$

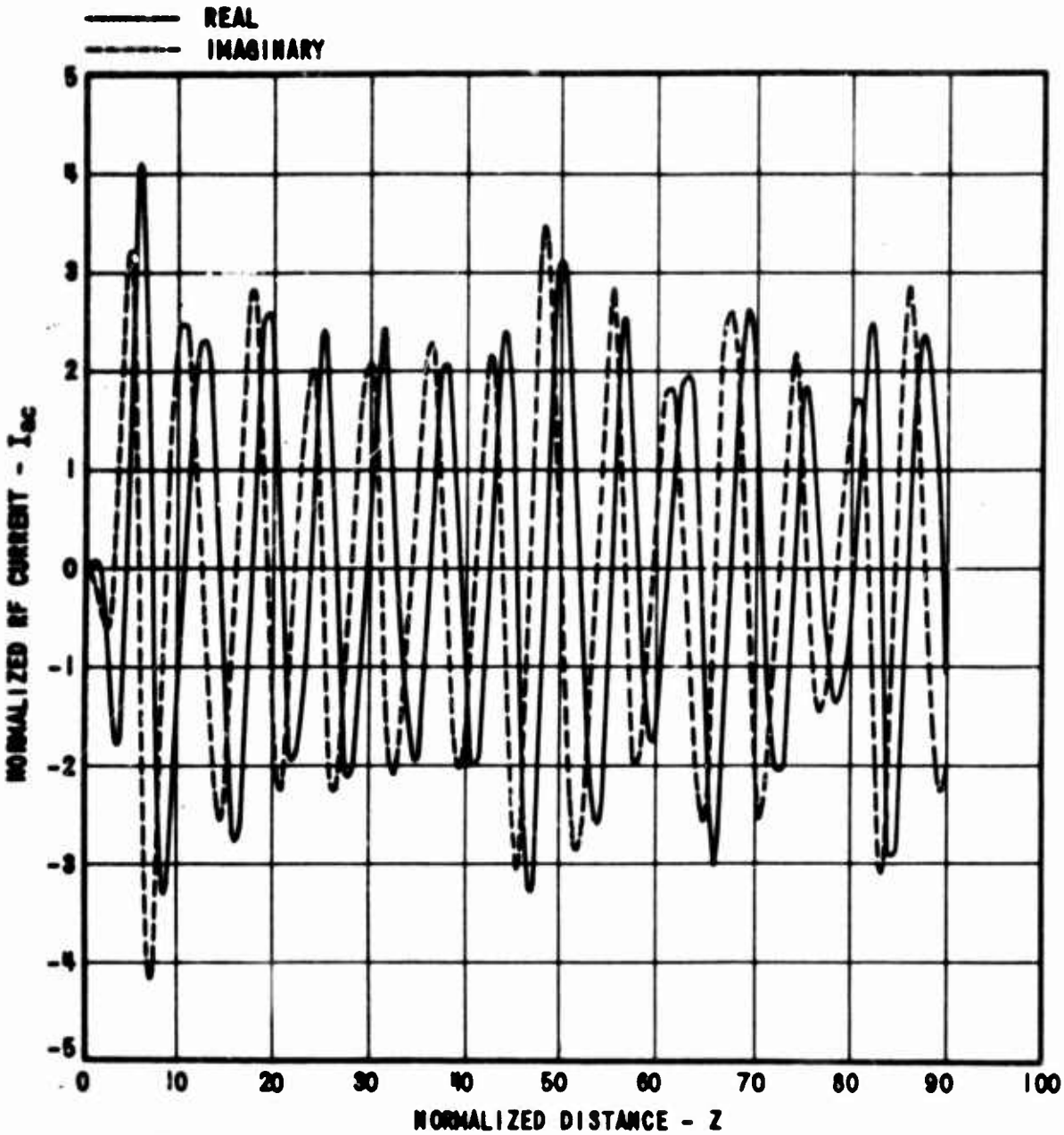

FIGURE A-1 NORMALIZED RF CURRENT

APPENDIX B

THE EFFECT OF SPACE-CHARGE UPON THE OPERATION OF THE PHASE SHIFTER

The analysis of the operation of the phase shifter has been made, using ballistic equations of motions. The effects of electron space-charge have not been included. It will be shown in this section that the space-charge introduces a correction to the preceding equation that results in a minor decrease in phase shift with no fundamental change in the operation.

The electron space charge will accumulate in the electron bunch to form an electric field which opposes the formation of the bunch. The initial current bunch must then be produced somewhat further away from the beginning of the slow-wave structure than in the ballistic case. For conventional values of space charge density, this change is small, being of the order of 10% in klystrons. An analytical analysis was made including space charge in the short phase shifter and the result was the same. The first current bunch formed later but it was of the same amplitude. Since the short phase shifter is relatively unimportant, only the results of the analysis will be presented. Equation (30) indicates that the bunching parameter for a short phase shifter may be approximated as $1/2\ cZ^2$ for $X < 3$. When space charge is included in the analysis, the new bunching parameter, X', becomes

$$X' = \frac{1}{2}\ cZ^2 \left[\frac{\sin\left|\frac{\omega_q Z}{2\omega}\right|}{\frac{\omega_q Z}{2\omega}} \right]^2 \qquad \text{(B-1)}$$

as long as $cZ \ll 1.0$, where $\frac{1}{2\pi}\ \omega_q$ = the reduced plasma frequency. A simple method of including this effect is to say the length Z is effectively reduced by space-charge to the value Z', where

$$Z' = \frac{Z \sin\left|\frac{\omega_q Z}{2\omega}\right|}{\frac{\omega_q Z}{2\omega}} \qquad \text{(B-2)}$$

Since most phase shifters will be long devices, Equation (B-2) does not apply and such initial effects are miniscule.

The most important effect of space charge must then be its effect upon the ac current in the remainder of the slow-wave structure. In particular, bunched electrons will produce an electric field which will oppose further bunching and reduce the phase shift. An estimate of the magnitude of this reduction can be made.

Maxwell's equation for the continuity of total ac current in one dimension gives

$$\frac{\partial}{\partial z}\ (J_z(z,t) + \dot{D}_z(z,t)) = 0 \qquad \text{(B-3)}$$

where

J_z = ac electron current density

D_z = displacement = $\epsilon_o E_z$

The bracketed quantity in Equation (B-3) can be thought of as the equivalent displacement current, $\dot{D}_z'(z,t)$, for an equivalent zero space charge case. The displacement current due to space charge, $\dot{D}_{sc}(z,t)$, is then just

$$\dot{D}_{sc}(z,t) = \dot{D}_z'(z,t) - \dot{D}_z(z,t) = J_z(z,t)$$

or

$$\frac{\partial E_{sc}(z,t)}{\partial t} = \frac{J_z(z,t)}{\epsilon_o} \ . \qquad \text{(B-4)}$$

For a beam of cross-sectional area A, Equation (B-4) becomes

$$\frac{\partial E_{sc}(z,t)}{\partial t} = \frac{i(z,t)}{A\,\epsilon_o} \quad . \tag{B-5}$$

Equation (B-5) shows that ac beam current at the fundamental and harmonic frequencies will produce an equivalent space charge field at fundamental and harmonic frequencies. The only electric field component that will produce any appreciable effect is the fundamental frequency component. The fundamental current component is

$$i(z,t) = -\frac{I_1}{2}\, e^{j(\omega t - \beta_o z)} - \frac{I_1^*}{2}\, e^{-j(\omega t - \beta_o z)} \tag{B-6}$$

so that integration of equation (B-5) produces

$$E_{sc}(z,t) = -\frac{1}{j^2 A\omega\epsilon_o}\left[I_1 e^{j(\omega t - \beta_o z)} - I_1^*\, e^{-j(\omega t - \beta_o z)}\right] \tag{B-7}$$

which can be rewritten as

$$E_{sc}(z,t) = -\frac{I_o}{A\omega\epsilon_o}\left[\mathrm{Re}\left(\frac{I_1}{I_o}\right)\sin(\omega_o t - \beta_o z) + \mathrm{Im}\left|\frac{I_1}{I_o}\right|\cos(\omega_o t - \beta_o z)\right]. \tag{B-8}$$

Using the following relations

$$\omega_p^2 = \frac{\frac{|e|}{m_e}\, I_o}{u_o\, A\, \epsilon_o} \tag{B-9}$$

$$2\,|e|\,V_o = m_e\, u_o^2$$

$$\beta_o = \frac{\omega}{u_o} \quad ,$$

the fractional quantity in Expression (B-8) can be rewritten as

$$\frac{I_o}{A \omega \epsilon_o} = 2 V_o \beta_o \left(\frac{\omega_p}{\omega}\right)^2 . \qquad \text{(B-10)}$$

Equations (B-8) and (B-10) can be made to include radial effects by replacing ω_p by ω_q which is ω_p times the plasma frequency reduction factor. The result is

$$E_{sc}(z,t) = -2 V_o \beta_o \left(\frac{\omega_q}{\omega}\right)^2 \left[R_e\left(\frac{I_1}{I_o}\right) \sin(\omega t - \beta_o z) + Im\left(\frac{I_1}{I_o}\right) \cos(\omega t - \beta_o z) \right] . \qquad \text{(B-11)}$$

The total equivalent circuit field is then approximately just the sum of $E_{sc}(z,t)$ and the "cold" circuit field, $- E_o \sin(\omega t - \beta_o z)$.

For $Z > 20$ radians, the computer solution for $c = 0.10$ shows that

$$Re\left(\frac{I_1}{I_o}\right) \approx 0.65$$

$$Im\left(\frac{I_1}{I_o}\right) \approx 0 , \qquad \text{(B-12)}$$

and $E_{sc}(z,t)$ is approximately

$$E_{sc}(z,t) \approx - 1.3 \beta_o V_o \left(\frac{\omega_q}{\omega}\right)^2 \sin(\omega t - \beta_o z) . \qquad \text{(B-13)}$$

The net circuit field is then approximately

$$E'(z,t) \approx - \left[1 + 1.3 \frac{\beta_o V_o}{E_o} \left(\frac{\omega_q}{\omega}\right)^2 \right] E_o \sin(\omega t - \beta_o z). \qquad \text{(B-14)}$$

Therefore, the major effect of space charge in long phase shifters is to produce an electric field which is of constant amplitude and in phase with the circuit field. The increase in electric field strength reduces the amount of phase shift obtained. For the usual values of operating parameters, the reduction is small (i. e. less than 10%). Since the total phase change is approximately inversely proportional to the electric field (Equation (53)), the phase change is reduced due to space charge multiplication by the factor

$$\left[1 + 1.3 \frac{\beta_o V_o}{E_o} \left(\frac{\omega_q}{\omega} \right)^2 \right]^{-1} \qquad \text{(B-15)}$$

This factor may then be applied to a ballistic computation to correct for the major effects of space charge. The correction is a reduction in phase shift which is usually less than 8%.

APPENDIX C

EVALUATION OF THE EMPIRICAL CONSTANT a

An earlier theoretical derivation of an expression for phase shift was given in the Final Report on the Research Program on the Electron Beam Phase Shifter (PT-815). Using field theory, and making certain assumptions as to the form of the ac current solution, it was shown that

$$\theta = a\, I_o\, \ell\, f \sqrt{\frac{K_c}{V_o P_{rf}}} \qquad \text{(C-1)}$$

where

a = empirical constant.

ℓ = circuit length in cm.

f = frequency in Gc.

Comparison of Equation (C-1) with Equation (54) of the text shows that

$$a = \frac{0.325 \times 10^9}{\sqrt{\frac{|e|}{m_e}}} \qquad \text{(C-2)}$$

which is

$$a = 24.2 .$$

Experimental values of a were usually close to 22, which indicates that the fundamental ac beam current has been accurately approximated.

APPENDIX D

HARMONIC OUTPUT POWER

Because the beam saturates very close to the beginning of the slow-wave structures, the beam will have a large harmonic current content which will probably be maintained over the greater portion of the interaction region. Harmonic power will be built up on the circuit if the circuit wave associated with the harmonic frequency has appreciable interaction impedance and a phase velocity not too different from that of the fundamental frequency, as is the case of the helix. In this case the harmonic power will increase toward the output end. For usual design values, the circuit harmonic power will not cause significant rebunching of the beam, and the bunching due to the drive power will dominate. (Because the harmonic power is quite low over most of the length of the tube, whereas the fundamental (drive) power is large throughout the tube.)

An estimate of the harmonic current present for the conditions as shown in the text is then obtained from Equation (6). For example, the second harmonic current is

$$I_2 = \frac{I_o}{\pi} \int_{-\pi}^{\pi} e^{-j2(T-Z)}\, dT, \qquad \text{(D-1)}$$

$$I_2 = I_{-2}^{*} .$$

The computer solution for electron trajectories could be used to obtain a computor calculation of the harmonic currents as a function of Z, but this has not been done. By using the analytical expression for T-Z given in section 4.0

$$T-Z \approx T_s - \frac{\sin T_s}{2} cZ^2 + \frac{\sin^2 T_s}{2} c^2 Z^3 , \qquad \text{(D-2)}$$

the analytical evaluation of the current integrals produces the following results for short devices:

$$\frac{I_1}{I_o} \approx e^{-jY} \left\{2J_1(X) + jY \left[-J_1(X) + J_3(X)\right]\right\}$$

$$\frac{I_2}{I_o} \approx e^{-j2Y} \left\{2J_2(2X) + j2Y \left[J_o(2X) + J_4(2X)\right]\right\}$$

$$\frac{I_3}{I_o} \approx e^{-j3Y} \left\{2J_3(3X) + j3Y \left[J_1(3X) + J_5(3X)\right]\right\} , \qquad \text{(D-3)}$$

where X and Y are defined in Equation (29). Figure D-1 shows the harmonic current amplitudes given by Equation (D-3) for the case of $c = 0.05$. It is evident that the harmonic current amplitudes build up to levels nearly the same as the fundamental current. Further, hand calculation verifies the fact that the harmonic current amplitudes are maintained for large values of Z (for example, at $Z = 31.4$ radians, $c = 0.10$, $\left|I_2/I_1\right| = 0.6$, $\left|I_3/I_1\right| = 0.62$).

It is worthwhile to estimate the second harmonic output, assuming "worst case" conditions. The circuit equation for harmonic interaction in a helix circuit is

$$\frac{d^2E_2}{dz^2} + \beta_2{}^2 E_2 = j\beta_2{}^3 K_2 i_2 \qquad \text{(D-4)}$$

where

E_2 = electric field component at second harmonic for slow wave structure

K_2 = Pierce's coupling impedance for second harmonic

β_2 = propagation constant at second harmonic for circuit and harmonic beam current.

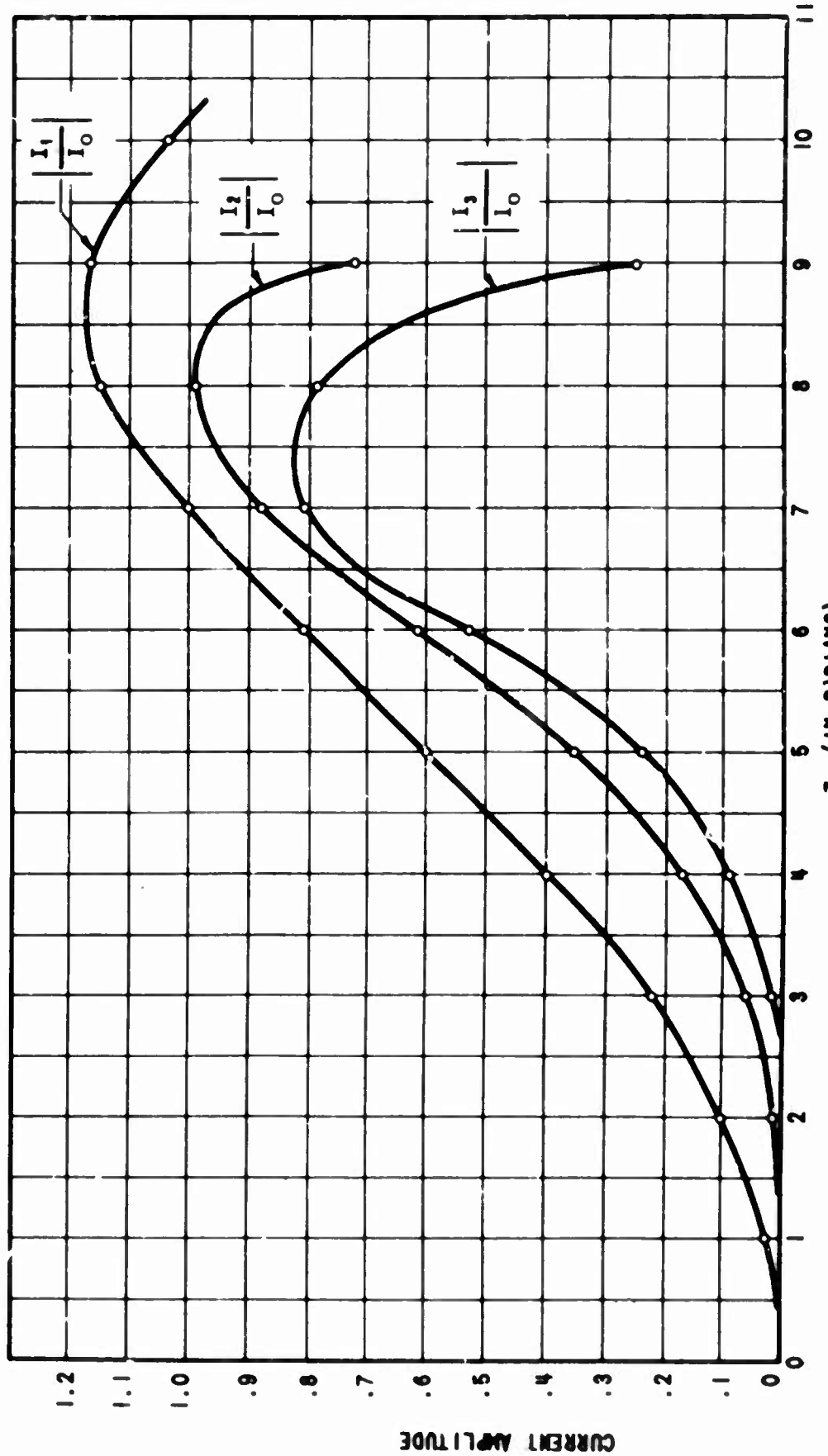

FIGURE D-1 Calculated Harmonic Current Amplitude for Phase Shifter with c = .95

It will be assumed that

$$\beta_2 \approx 2\beta_o$$

Equation (D-4) then becomes

$$\frac{d^2E_2}{dZ^2} + 4E_2 = j\,8\beta_o K_2 i_2 \cdot \qquad \text{(D-5)}$$

Define

$$E_2 = A_2(Z)\, e^{-j2Z}$$

$$i_2 = -I_2(Z)\, e^{-j2Z} \qquad \text{(D-6)}$$

Substitution of these variables into Equation (D-5) gives

$$\frac{d^2A_2(Z)}{dZ^2} - 4j\,\frac{dA(Z)}{dZ} = -j\,8\beta_o K_2 I_2(Z) \qquad \text{(D-6)}$$

Assuming that the amplitude of the second harmonic circuit field is not changing too rapidly with Z then the second derivative may be set equal to zero and a single integration of Equation (D-6) gives

$$A(Z) \approx 2\beta_o K_2 \int_0^Z I_2(Z)\, dZ \cdot \qquad \text{(D-7)}$$

The harmonic circuit power is

$$P_2 = \frac{|A(Z)|^2}{2\beta_2^2 K_2} \qquad \text{(D-7)}$$

which with the previous results becomes

$$P_2 \approx \frac{K_2}{2} \left| \int_o^Z I_2(Z)\, dZ \right|^2 \qquad \text{(D-8)}$$

A crude estimate of this power is obtained by assuming the second harmonic current is about equal to 60% of the fundamental current and taking the integral of the fundamental circuit equal to $0.65\ Z\ I_o$ by Figure 4-2 or

$$\left| \int_o^Z I_2(Z)\, dZ \right| \approx 0.39\ Z\ I_o \qquad \text{(D-9)}$$

which gives

$$P_2 \approx 0.076\ K_2 Z^2\ I_o^2 \quad . \qquad \text{(D-10)}$$

and by a similar process, the third harmonic power is

$$P_3 \approx 0.076\ K_3\ Z^2\ I_o^2 \, , \qquad \text{(D-11)}$$

where K_3 is the interaction impedance for third harmonic.

Harmonic impedance rapidly decreases with harmonic number because the structure width becomes a large fraction of a wavelength. For a helix of $\beta_o a = 1.5$, it is estimated that

$$\frac{K_2}{K_1} \approx 0.08$$

$$\frac{K_3}{K_1} \approx 0.01$$

The normal operating conditions of the S-band phase shifter were

$$K_1 = 125\ \Omega$$

$$I_o = 0.8\ A$$

$$Z = 70 \text{ radians}$$

$$P_1 = 10 \text{ kw}$$

$$P_2 \approx 2.4 \text{ Kw} \text{ or } -6.2 \text{ db from } P_1$$

$$P_3 \approx 0.30 \text{ Kw} \text{ or } -15.2 \text{ db from } P_1 .$$

By studying the proportionalities in Equation (53) and Equation (D-10) it is seen that an increase in either dc current or circuit length will produce a proportional increase in phase shift but twice as much increase in harmonic power output. However, an increase in interaction impedance will increase both phase shift and harmonic power output proportionally. Therefore, a higher fundamental circuit impedance is desirable for less harmonic output in a helix type phase shifter.

REFERENCES

1. Winsor, D. L., Yacus, J., "An Electronic Microwave Phase Shifter," Paper presented at the Symposium on Electronically Scanned Array Techniques and Applications, Rome Air Development Center, April 15, 1964.

2. Hamilton, D. R., Klystrons and Microwave Triodes, New York, MIT Rad. Lab. Series, "Velocity Modulation and Klystron Bunching," Vol. 7, Chpt 9, pp. 201 - 247.

3. Beck, A. H. W., "Space-Charge Waves and Flow Electromagnetic Waves," New York, Pergamon Press, 1958, p. 222.

4. Pierce, J. R., Traveling Wave Tubes, New York, D. Van Nostrand, Inc, 1950, p. 17.

Unclassified

Security Classification

DOCUMENT CONTROL DATA - R&D

(Security classification of title, body of abstract and indexing annotation must be entered when the overall report is classified)

1. ORIGINATING ACTIVITY (Corporate author) Raytheon Company Microwave and Power Tube Division Waltham, Mass 02154	2a. REPORT SECURITY CLASSIFICATION Unclassified 2b. GROUP

3. REPORT TITLE

HIGH POWER S-BAND ELECTRON BEAM PHASE SHIFTER TECHNIQUE

4. DESCRIPTIVE NOTES (Type of report and inclusive dates)
Final Report, 15 Mar 65 - 15 Jul 66

5. AUTHOR(S) (Last name, first name, initial)
ST. JOHN, Dr. Grant

6. REPORT DATE	7a. TOTAL NO. OF PAGES	7b. NO. OF REFS
	106	8

8a. CONTRACT OR GRANT NO	9a. ORIGINATOR'S REPORT NUMBER(S)
AF30(602)-3663	
b. PROJECT NO 4506	PT 1101
c. Task No. 450602	9b. OTHER REPORT NO(S) (Any other numbers that may be assigned this report) RADC-TR-66-506
d.	

10. AVAILABILITY/LIMITATION NOTICES
This document is subject to special export controls and each transmittal to foreign governments or foreign nationals may be made only with prior approval of RADC (EMLI) GAFB, NY 13440.

11. SUPPLEMENTARY NOTES	12. SPONSORING MILITARY ACTIVITY
	Rome Air Development Center (EMATE) Griffiss AFB New York 13440

13. ABSTRACT

This report is a summary of work performed under the sponsorship of Rome Air Development Center (Contract AF30(602)-3663) to design and develop a breadboard model of a 100 kilowatt S-band phase shifter. The phase shifter utilizes an electron beam of input power much lower than the microwave power transmitted through the structure. The variable current beam interacts with the slow-wave structure to perturb the propagation constants of the combined beam and slow-wave structure system.

A model was constructed and operated at a 100 kilowatt power level. The performance of this model was limited by low beam current; however, measured performance was in excellent agreement with theoretical values.

From this work, it can be concluded that a device in S-band operating at a 100 kilowatt power level and providing 360° variation in phase shift is feasible. The physical size and relatively high insertion loss of such an electron beam phase shifter tend to make it unattractive in comparison with recently developed solid-state phase shifters.

DD FORM 1 JAN 64 1473

Unclassified

Security Classification

Unclassified

Security Classification

14 KEY WORDS	LINK A		LINK B		LINK C	
	ROLE	WT	ROLE	WT	ROLE	WT
Phase Shifter Variable Current Beam interacts with Slow Wave Structure						

INSTRUCTIONS

1. ORIGINATING ACTIVITY: Enter the name and address of the contractor, subcontractor, grantee, Department of Defense activity or other organization *(corporate author)* issuing the report.

2a. REPORT SECURITY CLASSIFICATION: Enter the overall security classification of the report. Indicate whether "Restricted Data" is included. Marking is to be in accordance with appropriate security regulations.

2b. GROUP: Automatic downgrading is specified in DoD Directive 5200.10 and Armed Forces Industrial Manual. Enter the group number. Also, when applicable, show that optional markings have been used for Group 3 and Group 4 as authorized.

3. REPORT TITLE: Enter the complete report title in all capital letters. Titles in all cases should be unclassified. If a meaningful title cannot be selected without classification, show title classification in all capitals in parenthesis immediately following the title.

4. DESCRIPTIVE NOTES: If appropriate, enter the type of report, e.g., interim, progress, summary, annual, or final. Give the inclusive dates when a specific reporting period is covered.

5. AUTHOR(S): Enter the name(s) of author(s) as shown on or in the report. Enter last name, first name, middle initial. If military, show rank and branch of service. The name of the principal author is an absolute minimum requirement.

6. REPORT DATE: Enter the date of the report as day, month, year, or month, year. If more than one date appears on the report, use date of publication.

7a. TOTAL NUMBER OF PAGES: The total page count should follow normal pagination procedures, i.e., enter the number of pages containing information.

7b. NUMBER OF REFERENCES: Enter the total number of references cited in the report.

8a. CONTRACT OR GRANT NUMBER: If appropriate, enter the applicable number of the contract or grant under which the report was written.

8b, 8c, & 8d. PROJECT NUMBER: Enter the appropriate military department identification, such as project number, subproject number, system numbers, task number, etc.

9a. ORIGINATOR'S REPORT NUMBER(S): Enter the official report number by which the document will be identified and controlled by the originating activity. This number must be unique to this report.

9b. OTHER REPORT NUMBER(S): If the report has been assigned any other report numbers *(either by the originator or by the sponsor)*, also enter this number(s).

10. AVAILABILITY/LIMITATION NOTICES: Enter any limitations on further dissemination of the report, other than those imposed by security classification, using standard statements such as:

(1) "Qualified requesters may obtain copies of this report from DDC."

(2) "Foreign announcement and dissemination of this report by DDC is not authorized."

(3) "U. S. Government agencies may obtain copies of this report directly from DDC. Other qualified DDC users shall request through _____."

(4) "U. S. military agencies may obtain copies of this report directly from DDC. Other qualified users shall request through _____."

(5) "All distribution of this report is controlled. Qualified DDC users shall request through _____."

If the report has been furnished to the Office of Technical Services, Department of Commerce, for sale to the public, indicate this fact and enter the price, if known.

11. SUPPLEMENTARY NOTES: Use for additional explanatory notes.

12. SPONSORING MILITARY ACTIVITY: Enter the name of the departmental project office or laboratory sponsoring *(paying for)* the research and development. Include address.

13. ABSTRACT: Enter an abstract giving a brief and factual summary of the document indicative of the report, even though it may also appear elsewhere in the body of the technical report. If additional space is required, a continuation sheet shall be attached.

It is highly desirable that the abstract of classified reports be unclassified. Each paragraph of the abstract shall end with an indication of the military security classification of the information in the paragraph, represented as *(TS)*, *(S)*, *(C)*, or *(U)*.

There is no limitation on the length of the abstract. However, the suggested length is from 150 to 225 words.

14. KEY WORDS: Key words are technically meaningful terms or short phrases that characterize a report and may be used as index entries for cataloging the report. Key words must be selected so that no security classification is required. Identifiers, such as equipment model designation, trade name, military project code name, geographic location, may be used as key words but will be followed by an indication of technical context. The assignment of links, rules, and weights is optional.

Unclassified

Security Classification